LASER & PHOTONICS REVIEWS
www.lpr-journal.org

Single-Particle Characterization by Elastic Light Scattering

*Andrey V. Romanov and Maxim A. Yurkin**

The field of light-scattering characterization of single particles has seen a rapid growth over the last 30 years largely due to the progress in measurement and simulation capabilities. In particular, several methods have been developed to reliably characterize various particles, described by a model with several characteristics, with geometric resolution significantly better than the diffraction limit. However, their development has been largely fragmentary, limited to specific experimental set-ups. To fill this gap, these lines of development are reviewed within a unified framework. While focusing on characterization algorithms themselves, the experimental aspects related to the isolation and measurement of single particles are also discussed. The existing characterization methods are divided into three classes. The widest class is that of model-driven methods based on solving parametric inverse light-scattering problems, using a direct inversion of a low-dimensional mapping, a nonlinear regression, or neural networks. Other classes include model-free reconstruction methods and data-driven classification methods. This review is designed to be extensive in including all relevant literature, but the discussion of semi-quantitative imaging methods, such as tomography or holography-based reconstruction, is deliberately omitted. Throughout the review the development of various characterization methods is described, they are critically compared, and promising directions of future research are highlighted.

1. Introduction

Light scattering (more generally, interaction of electromagnetic waves with particles) is one of the most common methods for non-invasive analysis and characterization of various kinds of objects. It is successfully used in a wide range of applications in astrophysics, meteorology, biophysics, nanotechnology, and other fields. There exist a lot of experimental modalities, which can be divided into two broad classes. Inelastic scattering includes various kinds of spectroscopy, that is, wavelength-resolved measurements of absorption[1] or Raman scattering,[2] including angle-resolved ones.[3] Elastic light scattering (ELS) techniques imply that the wavelength of the incident radiation is not changing, hence corresponding measurements are typically performed at a single or a few wavelengths. Importantly, the ELS measurements can be fully described in the framework of the frequency-domain Maxwell's equations.[4,5]

Another important feature of characterization techniques is whether they apply to single particles or ensembles of particles (e.g., suspensions). The ensemble methods are naturally simpler on the experimental side due to a higher signal-to-noise ratio and trivial sample preparation. Thus, they were first to appear,[6,7] are used in many commercial instruments,[8,9] and in some cases are implicitly assumed for the whole field of optical particle characterization. However, restoring the distribution of the ensemble over characteristics is a notoriously ill-posed inverse problem, which can be solved reliably only if some prior information about this distribution is assumed. Single-particle measurements, while more technically complicated, are free of this limitation and allow reaching much better precision.[10,11]

This review is dedicated specifically to the characterization techniques based on the ELS measurements of single particles. In doing so we mostly focus on the near-optical part of the spectrum (from infra-red to shorter wavelengths), since at the microwave frequencies the scattering measurements are somewhat easier, for example, due to straightforward measurement of the wave phase.[12] Moreover, other physical phenomena can be described in the same classical ELS framework, for example, the electron-energy-loss spectroscopy[13,14] and (angle-resolved) cathodoluminescence,[15] but they are outside the scope of this review.

Two major prerequisites for development of single-particle characterization methods are the measurement and simulation techniques. The measurement techniques evolved from a single[16,17] or several discrete signals[18–20] to pseudo-continuous 1D[21–23] and 2D light scattering patterns (LSPs) in wide angular ranges.[24,25] The systems measuring 2D LSPs include holographic[26] and interferometric (phase-sensitive) ones,[27] as well as tomographic systems varying the incident direction.[28] The advancement of experimental systems has been recently reviewed by Kinnunen and Karmenyan.[29] The simulation methods have evolved from the Lorenz–Mie (LM) theory for spherical particles[30] to surface-[31] and volume-discretization methods,[32,33] applicable to arbitrarily shaped homogeneous and inhomogeneous particles, respectively.[34,35] Currently, arbitrary

A. V. Romanov, Dr. M. A. Yurkin
Voevodsky Institute of Chemical Kinetics and Combustion SB RAS
Institutskaya Str. 3, Novosibirsk 630090, Russia
E-mail: yurkin@gmail.com
A. V. Romanov, Dr. M. A. Yurkin
Novosibirsk State University
Pirogova Str. 2 Novosibirsk 630090, Russia

The ORCID identification number(s) for the author(s) of this article can be found under https://doi.org/10.1002/lpor.202000368

DOI: 10.1002/lpor.202000368

particles with sizes up to tens of wavelengths can be simulated with well-controlled accuracy, however, the simulations are not necessarily fast enough for all applications.

In addition to these numerically exact methods, there exist many approximate ones. Various weak-scattering approximations (such as Born or Rytov ones[36,37]) make the scattered field linear in the optical-contrast function (or the distribution of the refractive index inside the particle). Given sufficient experimental data, this linearity in principle allows reconstruction of the whole particle morphology. This forms the basis of a huge field of tomography.[28,38–41] Similarly, various scalar diffraction approximations are used in holography to reconstruct the 2D projection of the particle.[42,43] However, due to the used approximations and regularization during a reconstruction, both tomography and holographic reconstructions belong to the class of imaging methods, producing the 2D or 3D image of the object, which are at best only semi-quantitative. In other words, it is impossible to control the accuracy of these images or to use them for a precise estimation of geometrical characteristics. In this respect, they are similar to various microscopic techniques,[44,45] and we do not discuss them in this review.

By contrast, this review focuses on the characterization of single particles without employing approximations, which leads to the nonlinear inverse light-scattering problems (ILSPs), typically using shape models described by several characteristics. The solution methods for ILSPs is the third major prerequisite for characterization methods, which has seen a rapid growth over the last 30 years together with measurement and simulation capabilities. However, the development of ILSP solutions has been largely fragmentary, limited to specific experimental set-ups. These separate lines of developments include characterization of biological cells from 1D LSPs measured by the scanning flow cytometer,[46–48] characterization of aerosol particles from 2D LSPs measured with ellipsoidal reflectors,[25,49] and classification of biological cells in flow from 2D LSPs (diffraction images).[50,51] Moreover, a branch of holography has been developed into a characterization method,[52–54] by treating the holograms as 2D LSPs instead of applying approximate reconstruction. The main goal of the review is to describe the existing single-particle characterization methods, including the solution of ILSPs, in a unified framework. Thus, we highlight similarities in the existing methods for different experimental set-ups and describe promising cross-combinations for further development.

We start with a concise theoretical background in Chapter 2, followed by a review of existing experimental approaches to isolate single particles and to measure light scattering in Chapter 3. Chapter 4 is the core of the review, discussing in details all existing characterization methods. The largest attention is paid to model-driven methods, boiling down to solving the parametric ILSP (Section 4.1). But we also discuss reconstruction (model-free) methods in contrast to approximate tomography or holography approaches (Section 4.2) and data-driven classification methods (Section 4.3). Chapter 5 provides a conclusion and future perspective.

2. Theory

In this chapter, we briefly describe the theory behind light scattering. Extensive literature already exists on this subject;[4,5,55,56] our goal here is only to highlight basic definitions to simplify the discussion in further chapters. We consider a particle illuminated by a plane wave with the intensity I_{inc} and the free-space wavelength λ in a non-magnetic and non-absorbing host medium with the refractive index (RI) n_0. The wave vector in this medium is then $k = 2\pi n_0/\lambda$. For any particle one can introduce a generalized diameter (further denoted as the size d) as the maximum distance between two points inside the particle. In that case the dimensionless size parameter, roughly the ratio of the diameter to the wavelength, is defined as

$$x = kd/2 \tag{1}$$

Alternatively, the volume-equivalent diameter and the size parameter can be employed, corresponding to that of a sphere with the same volume as a given particle.

Another important parameter is the phase shift ρ (of the wave in the particle as compared to the host medium), defined as

$$\rho = 2x\,(m-1) \tag{2}$$

where $m = n/n_0$ is the relative RI of a particle. Strictly speaking, this definition is valid only for homogeneous spheres, but it is also meaningful for other particles if using any of the above definitions for x and some average of RI. Moreover, if m is complex (absorption is present), it is commonly replaced by $\mathrm{Re}\,m$ in Equation (2) to keep ρ real. Both x and ρ are commonly compared against unity for a definition of different regimes, where certain approximations are valid for light-scattering simulations (see, e.g., Section 4.1).

The total scattered power P_{sca} is proportional to the incident intensity as

$$P_{\text{sca}} = C_{\text{sca}} I_{\text{inc}} \tag{3}$$

where C_{sca} is the scattering cross-section. The same is true for absorption (P_{abs} and C_{abs}), while the extinction (power removed from incident radiation) is the sum of the above

$$\begin{aligned} P_{\text{ext}} &= P_{\text{sca}} + P_{\text{abs}} \\ C_{\text{ext}} &= C_{\text{sca}} + C_{\text{abs}} \end{aligned} \tag{4}$$

where P_{ext} is the extinction power and C_{ext} is the extinction cross-section.

Far from the particle, which is placed around the origin, the scattered radiation appears as a spherical wave, whose electric-field components are linearly related to that of the incident field at the same point $\mathbf{r}$ ("sca" and "inc" subscripts, respectively)

$$\begin{pmatrix} E_{\parallel \text{sca}} \\ E_{\perp \text{sca}} \end{pmatrix} = \begin{pmatrix} S_2 & S_3 \\ S_4 & S_1 \end{pmatrix} \frac{\exp\left[\mathrm{i}k\,(r-z)\right]}{-\mathrm{i}kr} \begin{pmatrix} E_{\parallel \text{inc}} \\ E_{\perp \text{inc}} \end{pmatrix} \tag{5}$$

where indices $\parallel$ and $\perp$ denote components parallel and perpendicular to the scattering plane, respectively, $r = |\mathbf{r}|$, z is its z-component, and $\exp(-\mathrm{i}\omega t)$ time dependence of harmonic waves is assumed (ω is the wave frequency). S_{1-4} are the components of the amplitude scattering matrix, which generally depend on the scattering direction $\mathbf{r}/r$, or spherical angles θ and φ, and are determined by the particle geometry and composition.

In practice, detectors measure the intensity of the electric field averaged over the time of a measurement, which is in most cases much larger than $1/\omega$. The most natural quantities for such measurement are the four Stokes parameters defined as follows

$$\begin{aligned} I &= \frac{\varepsilon_0 c n_0}{2}\left(E_\parallel E_\parallel^* + E_\perp E_\perp^*\right) \\ Q &= \frac{\varepsilon_0 c n_0}{2}\left(E_\parallel E_\parallel^* - E_\perp E_\perp^*\right) \\ U &= \frac{\varepsilon_0 c n_0}{2}\left(E_\parallel E_\perp^* + E_\perp E_\parallel^*\right) \\ V &= \frac{\varepsilon_0 c n_0}{2}\left(E_\parallel E_\perp^* - E_\perp E_\parallel^*\right) \end{aligned} \tag{6}$$

where $*$ denotes the complex conjugation and the constant factor, including the vacuum permittivity ε_0 and the speed of light c (related to the SI system of units), is frequently omitted if only relative intensities are considered. The incident and scattered Stokes vectors are also linearly related through the Mueller (or Stokes) scattering matrix

$$\begin{pmatrix} I_{\text{sca}} \\ Q_{\text{sca}} \\ U_{\text{sca}} \\ V_{\text{sca}} \end{pmatrix} = \frac{1}{k^2 r^2}\begin{pmatrix} M_{11} & M_{12} & M_{13} & M_{14} \\ M_{21} & M_{22} & M_{23} & M_{24} \\ M_{31} & M_{32} & M_{33} & M_{34} \\ M_{41} & M_{42} & M_{43} & M_{44} \end{pmatrix}\begin{pmatrix} I_{\text{inc}} \\ Q_{\text{inc}} \\ U_{\text{inc}} \\ V_{\text{inc}} \end{pmatrix} \tag{7}$$

The elements of the Mueller matrix M_{ij} can be expressed through that of the amplitude matrix.[4] If no polarizer is used before a detector, it measures I_{sca} integrated over the detector aperture. If additionally the incident field is not polarized ($Q_{\text{inc}} = U_{\text{inc}} = V_{\text{inc}} = 0$), I_{sca} is determined solely by the M_{11} element, also known as the phase function.

In digital holography the interference between the incident and scattered radiations takes place[42,57]

$$I_{\text{meas}}(\mathbf{r}) = \frac{\varepsilon_0 c n_0}{2}\left|\mathbf{E}_{\text{inc}}(\mathbf{r}) + \mathbf{E}_{\text{sca}}(\mathbf{r})\right|^2 \tag{8}$$

When measuring this intensity in the plane $z = z_0$ at some distance behind the object (assuming propagation along the z-axis), the problem resemble diffraction, for which a number of approximations are available. Importantly, they all consider a 3D particle only through its transmission function $t(x, y)$, which defines the total field at a plane $z = z_1$ immediately after the particle

$$\mathbf{E}(x, y, z_1) = \mathbf{E}_{\text{inc}}(x, y, z_1)\, t(x, y) \tag{9}$$

which by itself implies the scalar field approximation (i.e., the field polarization is not changed by the particle). Under the same approximation the total field at the measurement plane $\mathbf{E}(x, y, z_0)$ is linearly related to $\mathbf{E}(x, y, z_1)$ by a diffraction integral.

Inverting the latter can provide $t(x, y)$, which is generally expressed as

$$t(x, y) = \exp\left[-a(x, y)\right]\exp\left[\mathrm{i}\phi(x, y)\right] \tag{10}$$

where $a(x, y)$ describes absorption and $\phi(x, y)$—phase shift introduced by the object. While either of these two functions can be considered an image of the object, it is generally not suitable for precise characterization. Only for weakly scattering particles, it is rigorously related to the particle thickness $h(x, y)$ along the z-axis

$$t(x, y) = \exp\left[\mathrm{i}k(m - 1)\, h(x, y)\right] \tag{11}$$

where the integral of $m(\mathbf{r}) - 1$ along the z-axis should be used for inhomogeneous particles. Equation (11) is also used in the anomalous diffraction (AD) approximation.[55]

3. Available Techniques

This chapter describes various experimental techniques to obtain an optical signal from single particles, since instrumental limitations largely determine the feasible characterization approaches. There are two main issues for any single-particle measurement system: isolating particles and measuring their signals, both are discussed separately below. Fundamentally there are three ways to isolate particles, related to a sample, a flow, and a trap. In real applications they can be combined, but we consider them separately to highlight the relation between this choice and the measurable signals.

The sample approach is the simplest and the most common one applied from the very beginning of microscopy. Typically, a sample is a substrate with sedimented particles or a diluted suspension in a cuvette, so that the influence of particles on each other (multiple scattering) can be neglected. The same approach is implemented in multiparticle (sample-averaged) scattering systems, that is, to measure the average extinction cross section from the measured optical density. To obtain single-particle signals a small illumination volume is commonly used,[58] which in case of a suspension implies that particles only occasionally wander into it. The wide illumination can be kept in the case of a substrate,[17,59] while in the case of a suspension, only interferometric systems can afford the same[27] (discussed below). Overall, the sample approach is technically simple; however, difficulties arise in measuring light scattering due to limited space, for example, measuring only forward or backward scattering[42] in the case of a substrate, or due to the presence of noise in the case of a suspension.

The flow approach is based on hydrodynamic or aerodynamic focusing[60,61] for liquids or gases, respectively. In the simplest version, a stream of liquid or gas containing particles is combined with an external coaxial stream, thereby squeezing the inner stream and causing the particles to line up one after another in the resulting jet (with a sufficient inter-particle distance to guarantee the single-scattering regime). The advantage of this approach is the high particle throughput of up to 10 000 particles per second[62,63] and low spatial restrictions, allowing the efficient collection of the scattering signal from various directions (forward, backward, and side scattering, etc.). In addition, focusing technologies affect the spatial orientation of elongated particles in the flow,[64] which helps in solving inverse problems (see Section 4). The main disadvantage is inability to repeatedly measure the same particle, although holographic methods can partially circumvent this restriction[42] measuring along some interval in the stream.

The trap approach is based on capturing single particles in photophoretic,[65] electromagnetic,[66] or optical[67] traps (optical tweezers). It can accurately set the particle position, as

in the flow approach, but can additionally keep it for a long time, manipulating both the particle position and, with some limitations, its orientation.[68] In many applications such features are extremely desirable, similar to the full particle control in microwave-analogue experiments.[69,70] However, difficulties with practical implementation and limitations on particle characteristics hampered its widespread use. In particular, this affects biological particles in liquid, which have low relative RI unsuitable for intensity-based optical traps.[71] Moreover, this approach has a low throughput of less than one particle per second.

Measurement techniques are more diverse in their approaches, but we divide them into two classes of signals: discrete and continuous (angle-resolved). The first class involves measuring the scattering intensity integrated over a certain angular range by using a photomultiplier (PMT) or other detector, but there is no strict limit on the number of such scalar signals. We further denote this number as n. The second class involves a much larger n; together these measurements form a quasi-continuous signal with respect to the scattering angle—the so-called LSP. For instance, this can be achieved by using CDD cameras for 2D pattern or photodiode arrays for 1D. The main difference between these two classes lies in the amount of collected information and, hence, in its use at the analysis (inverse-problem) stage. Let us take a closer look at the representatives of each of these classes.

A huge number of instruments measure discrete light-scattering signals due to the ease of implementation. The optical setups measuring one,[16,72–75,17,59] two,[18,76,77] three,[19,78] four[20,63,79] signals are widespread. Some variation is observed in the types of signals: the common forward[19] and side[17,59,75,80,81] scattering, integrated intensity in some specific solid angle[20,74,78] or spherical angles ranges,[16,18,76] sometimes optimized to solve the necessary problem.[18,76] Also polarizing elements[20] and multi-wavelength setups[19,79] were used, which increase the number of signals. Combinations of all of the above create a variety of measurement approaches.

The single particle optical extinction and scattering (SPES) method developed by Potenza et al.[82,83] should also be attributed to this class, although it measures a 2D interference pattern (similar to digital holography below). The whole measurement is compressed into two values: the real and imaginary part of the scattered amplitude at the exact forward direction, which can further be transformed into C_{ext} and the phase-shift cross section (the latter is related to ρ) using the optical theorem.[4,55] The advantages of the SPES in the ability to characterize particles ranging in size from 100 nm to several microns, but the requirement of strong scattering hampers its application to particles with low relative RI, such as biological objects.

The continuous-signal techniques represent the pinnacle of light scattering measurements collecting a large amount of scattering information. The corresponding instruments can be divided into those measuring either 1D or 2D signal (1D and 2D LSPs, respectively), since their approaches to both characterization and measurement are significantly different.

Commonly, 1D LSP is obtained by either a rotating PMT (combined with a trap) or an array of photodiodes or PMTs. For example, Ray *et al.*[84] measured LSPs of spheres in an electrodynamic trap from 35° to 55° with a photodiode array or from 66° to 106° with a rotating PMT. Doornbos et al.[71] used a rotating

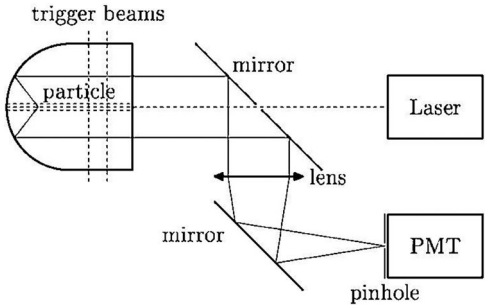

Figure 1. The SFC optical scheme. Reproduced with permission.[94] Copyright 2008, IOP Publishing.

PMT to record scattering of an optically trapped human lymphocyte. A similar goniometric system was used in a scattering measurement of a two-beam optically trapped red blood cell with controlled orientation.[68] Nakagawa et al.[85] described a multi-detector single-particle nephelometer (a detector array installed around the test space) in air flow with the throughput of ten particles per second and the instrument function accounting for particle movement. The low angular resolution of such devices hampers measurement of particles larger than 20 μm, and they found application mostly in the study of atmospheric phenomena.[86–88]

Alternative methods employ a single PMT to measure scattering intensity in a time-resolved manner at the cost of a reduced throughput. For example, Zhang et al.[22] measured the scattering intensity of a particle flying through a Gaussian beam and showed the proportionality of the parameters of the resulting scattering pulse to the particle size, which corresponds to forward or side scattering from the previous examples.

Truly 1D-LSP measurement with a single PMT was achieved by a scanning flow cytometer (SFC).[46,89] In this instrument the particle moves along the axis of a hemispherical mirror, which reflects only some rays exactly along the axis (which are further collected by a pinhole before the PMT). This collection scattering angle changes with particle position; thus, measured signal as a function of time has one-to-one correspondence to the scattered intensity as a function of the polar angle θ (**Figure 1**). The SFC allows one to obtain the scattering intensity, averaged over the azimuthal angle φ, for values of the polar angle θ from 10° to 70°[90] at a throughput of up to 200 particles per second.[91] Later the SFC was improved by measuring polarized LSPs to detect particle non-sphericity[92] and by simultaneous measurements of forward and side scattering for extremely precise characterization of homogeneous spheres.[93]

In the vast majority of cases, 2D LSPs are measured using CCD matrices. Three existing approaches differ in the following features: the presence of partial or complete focusing of the scattered radiation and the presence of interference with the incident field. While all of these can be used in a flow, the existing exposure time commonly reduces the throughput to a few particles per second to avoid blurring.[78,95–97] However, there are rare examples of the throughput of up to 1000 particles per second.[98,99]

The diffraction imaging technique[99,101,102] is based on measuring angle-resolved side scattering in a wide solid angle centered at 90° with a half-cone angle of about 25°[50] using a CCD matrix (**Figure 2**). Due to high CCD exposure time, the stream

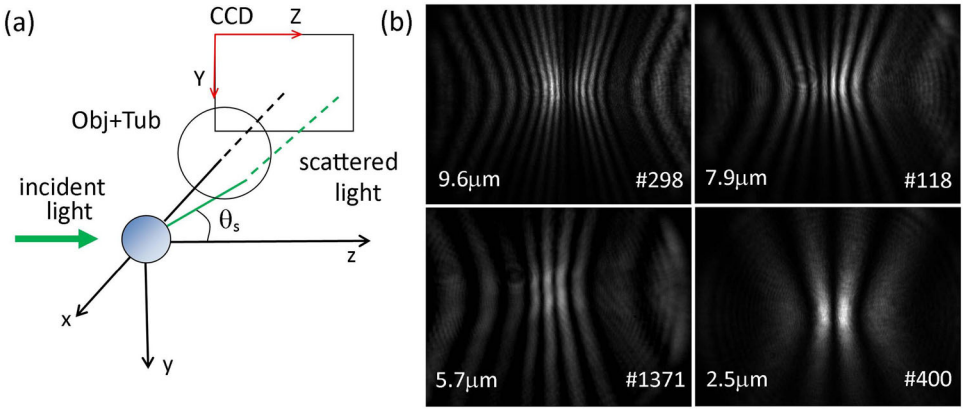

Figure 2. Typical scheme of a) a diffraction imaging configuration and b) obtained diffraction images of single polystyrene microspheres with nominal diameters shown on each image. Reproduced with permission.[100] Copyright 2012, The Optical Society.

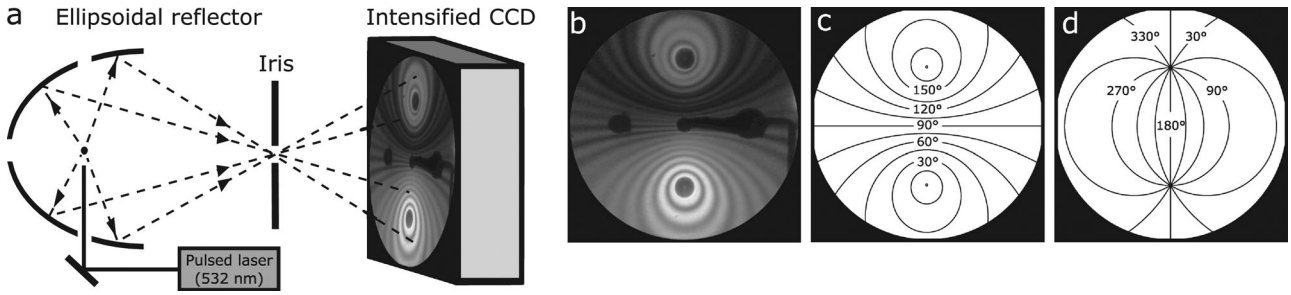

Figure 3. a) The optical scheme, b) scattering pattern, c) polar and d) azimuthal angular mapping for the TAOS system. Reproduced with permission.[25] Copyright 2019, Elsevier.

velocity has to be significantly smaller than in other flow methods, leading to a low throughput.[103,104] The method has been reliably applied to particles of tens of μm in size,[50,51,98,105–108] however, characterization for particle sizes from 1 to 100 μm has also been demonstrated.[100,109] Other side-scattering configurations include angular ranges: $79° < \theta < 101°$, $9° < \varphi < 31°$,[110,111] $88.3° < \theta < 91.7°$, $-117° < \varphi < 63°$,[112] and $86° < \theta < 94°$, $142° < \varphi < 168°$.[113] A similar optical scheme is used in the small-angle light scattering (SALS), where a CCD camera measures forward scattering from 2° to 30°[97,114–116] or from 6° to 25°.[117,118]

An analogous approach is applied in interferometry, where the scattered field is focused, but is measured out of the focus plane,[27,119–123] leading to microscopic-like image with interference fringes as the main information source.

The above 2D-LSP techniques rarely cover a wide angular range of more than 30° of the polar angle. This limitation was circumvented with the help of ellipsoidal mirrors, leading to the measurement of 2D angular optical scattering (TAOS) (**Figure 3**). Such system was applied to atmospheric aerosol particles, measuring scattering in ranges $75° < \theta < 135°$ and $0° < \varphi < 360°$.[25,124–127] Sindoni[128] applied a similar instrument to biological spores for even wider range of polar angle $15° < \theta < 165°$.

Another option to measure 2D LSPs, is Fourier-transform light scattering (FTLS).[129,130] It is based on measuring the amplitude and phase of the scattered field in the image plane of the object, which is further numerically propagated into the scattering (far-field) plane. It requires high spatial coherence of the incident beam and high accuracy of the phase measurement performed with an interferometer. The method was applied to various biological cells;[131–135] in particular, it was used for characterization of red blood cells using the Born approximation (for light-scattering simulations).[36] However, application of the FTLS to characterization of single particles is questionable, since the numerical propagation does not add any new information, but requires additional computations and distorts the experimental noise. In other words, fitting the measured complex field in the image plane may be more robust than fitting the corresponding 2D LSP.

One of the most powerful techniques of measuring the interference between the scattered and the incident fields is the digital in-line holography (DH)[42,136] (**Figure 4**). It requires a high spatial coherence of the incident beam and intense scattering. DH has been applied to characterization of polystyrene spheres,[52,137–140] milk fat globules,[138] asymmetrically coated spheres and rods,[53] *Escherichia coli*[95,141] spheres aggregates,[142] polymer-shelled microbubbles,[143] and protein aggregates.[144,145] There were also attempts of polarization measurements[146] and combination with independent light-scattering measurements.[147,148]

It is important to note that the reconstruction possibilities to obtain $t(x, y)$ within the framework of the scalar diffraction approximations (see Chapter 2 and Section 4.2) served as a catalyst for the development of DH, combining various options

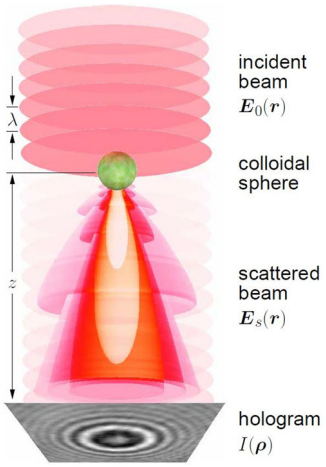

Figure 4. Principle of digital holography. Reproduced with permission.[52] Copyright 2007, The Optical Society.

for implementing the interference of the reference beam and the scattered field. This led to such methods as quantitative phase imaging and quantitative phase microscopy, which are described in details in refs. [42,149].

Strictly speaking, any microscopic image can potentially be used for characterization of single particles through the solution of ILSP. This is complicated due to the relatively complex optical scheme and incoherent light sources. Anyway, this vast area requires a separate review. Here we only mention the works combining microscopy and direct scattering measurements. For example, Itzkan et al.[150] combined a typical confocal microscope with light-scattering spectroscopy. This system provided the size, shape, and RI measurements of particles smaller than the diffraction limit. Wilson et al.[151] conducted a detailed study to optimize the optical configuration of the microscope with dark-field illumination and cross-polarization to discriminate healthy and malaria-infected RBCs (the latter contain crystalline inclusions—hemozoin). Richter et al.[152] used an inverted microscope with variable-angle illumination to measure LSP by a single PMT. They applied light scattering for cell differentiation before and after apoptosis.

To conclude this section, we examined the main technical aspects of isolating single particles and measuring their light-scattering signals. At the moment, the most advanced technologies are based on flow and angle-resolved techniques, respectively. Combining the two allows one to obtain a large amount of accurate scattering information.

4. Characterization Methods and Inverse Problems

In this chapter we describe various approaches to characterization, that is, retrieving some information about an object from the scattering data assuming some prior information. Depending on the amount and type of the latter, different types can be defined: model-driven, reconstruction, and data-driven ones. In the most common model-driven case, the characterization boils down to solving the parametric ILSP since the prior information is expressed as a particle model described by several characteristics (parameters). The number of the latter is further denoted as p.

The reconstruction approach aims at obtaining the distribution of RI in space using as little prior information as possible. It also uses the largest volume of scattering data among all methods, but even then the solution is notoriously unstable and ambiguous, unless some approximations are assumed. However, these approximations impose restrictions on the size and/or RI of the object, which limits applicability of the methods and constitutes prior information by themselves.

In the data-driven approach, previously collected data serve as prior information and is used to construct a predictive model. Such methods perform classification and identification, which can be considered a specific case of characterization, where several continuous characteristics of a model are replaced by a single discrete value in the output. They are primarily developed for practical applications and are hard to generalize. However, their successes may indicate a hidden potential of more elaborate characterization techniques.

The classification of characterization methods, corresponding to the structure of this chapter, is shown schematically in **Figure 5** and highlights relations between these methods and the experimental approaches of Chapter 3.

4.1. Model-Driven

Solving a parametric ILSP always relies on the solution of the corresponding direct problem (simulation), either in real time or for building a precomputed dataset. There are several extensive reviews of various methods to simulate light scattering.[34,35,153] Importantly, the choice of an optimal method largely depends on the complexity of the particle model. For homogeneous or multilayered concentric spheres, the well-known LM theory is definitely the method of choice due to its speed, accuracy, and stability.[30,154] It is commonly considered an analytical method, although it is a specific case of the separation-variable method leading to a solution in terms of an infinite series. Anyway, it is the fastest numerically exact method taking around 1 ms per particle on a standard desktop. Already for spheroids the latter is not necessarily the best option due to stability issues.[155,156] In general, for axisymmetric homogeneous shapes the extended-boundary-condition method (EBCM), also known as the T-matrix method,[31,35] is most frequently used. And its extension, multi-sphere T-matrix (MSTM),[157] is commonly used for aggregates of spheres. The typical simulation times start from seconds, but increase to minutes and more for large and/or concave particles (with the T-matrix methods)[158,159] or large number of spheres (with the MSTM).[160] For more complicated and inhomogeneous shapes, volume-discretization methods, such as the finite-difference time-domain (FDTD) method[32] and the discrete dipole approximation (DDA),[33,161] are commonly employed. The corresponding simulation times start from minutes (seconds in rare cases) and increase unboundedly (requiring a compute cluster) with size and, in the case of the DDA, with the refractive index.[162,163] In addition to the above numerically exact methods, that is, those that can reach arbitrary good accuracy given sufficient computational resources,[164] there exist various approximations, for example, Rayleigh–Gans–Debye (RGD, also known as the Born approximation) and Wentzel–Kramers–Brillouin (WKB) approximations, geometric optics,

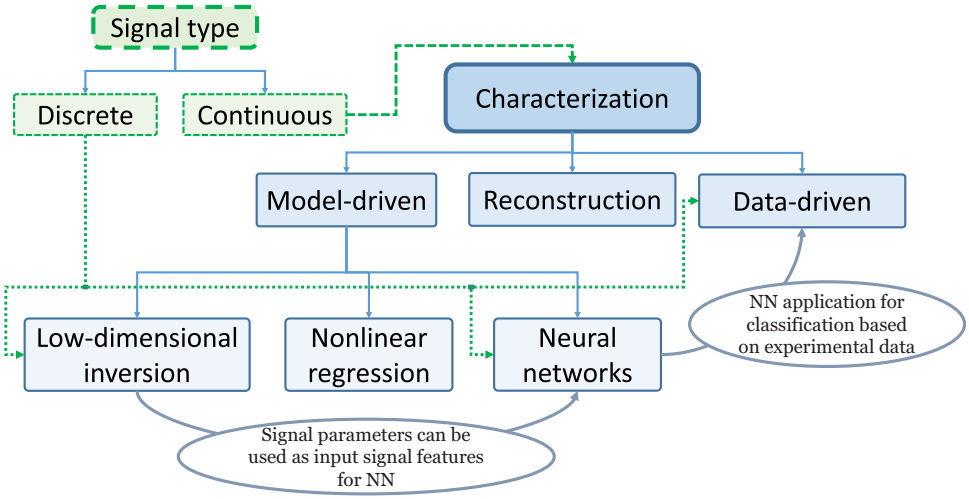

Figure 5. Classification of single-particle light-scattering characterization methods (shown in blue), proposed in this review, and their relation to experimental techniques (shown in green).

and Fresnel–Kirchhoff diffraction,[4,5,42,165] which may lead to truly analytical expressions in some cases.

A related issue is the adequacy of the shape model. In most cases a compromise is sought between the complicated morphology of actual particles and simplified models, aimed both at minimizing the number of free parameters and at enabling the use of less computationally demanding simulation methods. While in many applications various imaging (microscopic) techniques are used to support the model choice, the adequacy of the simplified models is then qualitatively discussed based on the comparison of simulated and measured LSPs. For example, Neukammer et al.[112] measured 2D LSPs (around the forward direction) for chains of up to five spheres in an optical trap and showed qualitative agreement with the interference-combined LM results for single spheres. Aptowicz et al.[124] demonstrated that the LM theory (i.e., a spherical shape model) may be adequate for most micron-sized urban aerosol particles but not for supermicron particles. Brock et al.[166] showed that a coated sphere is a poor approximation of a lymphocyte in the entire range of scattering angles, except for the near-forward direction. The reference shape of the lymphocyte was constructed from confocal images, and the FDTD was used for simulations. Moskalensky et al.[167] showed that multiple scattering of the optically soft monomers inside an aggregate can often be neglected.

Being the most common type of characterization, the model-driven approach is implemented in a wide variety of methods. We group them into three subclasses: low-dimensional inversion, nonlinear regression (fitting), and neural networks (NN).

4.1.1. Low-Dimensional Inversion

Historically, this is the very first type of methods corresponding to the instruments with discrete measured signals. However, these methods can also be used with continuous-signal instruments, if instead of a complete signal only a few derived parameters are used. In both cases the characterization boils down to inversion of a low-dimensional mapping from a set of particle characteristics, a subset of $\mathbb{R}^p$, to a set of signal parameters (or signals themselves), a subset of $\mathbb{R}^n$. The direct mapping $\mathbb{R}^p \to \mathbb{R}^n$ can often be calculated theoretically (by light-scattering simulations) allowing its detailed study due to low dimensionality.

Obtaining a unique and robust (noise-resistant) solution is of utmost importance, and in some cases the signals (or signal parameters) are explicitly selected to achieve this goal. In particular, Ackleson and Spinrad[81] studied curves of the constant size or RI in coordinates of experimental signals. More detailed analysis of 2D mappings ($\mathbb{R}^2 \to \mathbb{R}^2$), that is, two discrete signals versus size and RI, was performed to characterize RBCs.[18,76] Initially, the signals were chosen to obtain the maximum variation of LM theoretical values over the range of physiological values, then uniqueness of the mapping was verified. A similar analysis of uniqueness of a 2D mapping for spheres has been performed by Konokhova et al.[93]

The inverse mapping $\mathbb{R}^n \to \mathbb{R}^p$ is generally constructed by some kind of interpolation, which is straightforward for low dimensions. However, occasionally explicit formulas are obtained. For instance, a polynomial function of one signal was used by Flynn et al.[77] to estimate the size and RI of spheres in an optical trap. The polynomial coefficients depend on the other signal and were obtained from calibration measurements. Another example of interpolation-like approach is the overlapping confidence (measured) ranges of several signal parameters in coordinates of the size and RI, which allows obtaining a confidence range for these characteristics[168] (similar to that in Section 4.1.2).

The general advantages of low-dimensional inversion are high processing speed and the ability to investigate uniqueness and robustness in advance. The disadvantages are often the limited applicability range of both the model characteristics (e.g., for guaranteed uniqueness) and the models themselves (since $p \leq n$ and complexity of mapping inversion drastically increases with p and n). As a result, we are not aware of any examples of inverse mappings with $p > 2$.

An illustrative example is the SPES method, which measures the complex forward-scattering amplitude.[83] Originally, the 2D mapping inversion has been used for spheres[82] or

for particles approximated by spheres (nanoparticles with a drug payload).[169] Next, there were attempts to obtain some information about shape, such as the aspect ratio of a spheroid (assuming fixed RI)[170,171] or discrimination of aggregates from simpler shapes.[172] Those attempts lack the discussion of solution uniqueness for an individual particle, but employ statistical analysis of the obtained characteristics for the whole sample. Similar statistical arguments have recently led to retrieval of complex RI, shape (among several options), and the size distribution for particulate samples.[20] More specifically, the method assumes that the sample consists of several classes, and inside each class all particles has the same shape and complex RI. The resulting methods can be placed half-way between the single-particle techniques, discussed in this review, and the statistical (fluctuational) characterization methods for particle ensembles, such as dynamic light scattering.[173] Another recent extension of the SPES[174] combines it with intensity measurements at two scattering angles, but instead of a particle characterization the data is used to directly estimate the particle phase function.

By contrast, other researchers do not pursue a complete characterization but limit themselves to observing 1D correlation between a particle characteristic and a signal. This includes the particle size versus the scattering intensity,[80,127,175] the width of the scattering pulse (using a Gaussian beam),[22] or the forward to backward scattering ratio,[176] as well as the particle shape (aspect ratio) versus the asymmetry in 2D LSP[127,175,177] or two ratios of intensities at different wavelengths.[19] However, the proportionality coefficient generally depends on other particle characteristics (size, shape, and material). Hence, a separate calibration is required for each case.

The nanoparticle tracking analysis (NTA) technique[178] has also been extended to light-scattering characterization.[17,59] The authors used the maximum scattering intensity along with the known hydrodynamic diameter, determined by the NTA, to obtain the particle RI. Gardiner et al.[59] carefully discuss all limitations of the method, including the effect of sizing inaccuracy. However, no quantitative uncertainty estimates were given.

Another approach deserving separate consideration is the spectral one. It is based on the wave nature of light, manifesting itself in the oscillatory structure of LSPs, also related to the interference phenomenon. Although the corresponding methods start with a continuous LSP, only parameters related to its carrier frequency or oscillation period are used for particle characterization.

The approximate analysis was performed based on Fraunhofer diffraction[25,118,179] and on the interference between different orders of scattered radiation.[27,119–123] The observed LSP oscillation frequencies linearly depend on the particle size, which holds in the remarkably wide range of particle characteristics. The primary focus is then on high accuracy and precision of sizing under variation of remaining particle characteristics (RI, shape, etc.). However, the lack of a rigorous theory and instrumental limitations make this approach largely empirical. The only exception based on a rigorous theory is the work by Ludlow and Everitt.[180] They transformed the sphere's scattering intensity into the Gegenbauer spectrum and related the boundary frequency, after which the exponential decay begins, with the size (additionally estimating the RI from the spectrum). However, this solution requires an LSP to be measured in the whole angular range, which has not been implemented experimentally.

Direct-parametrization variants of the spectral approach focus on measuring distances between LSP peaks and valleys[119,120,123,181–183] or its locations[184] and relating them to the size. Shepelevich et al.[185] studied extrema location in an LSP under conditions of the WKB, RGD, Fraunhofer-diffraction, and AD approximations. They showed that the minima migrate monotonically with varying size and the distance between the minima is not sensitive to the RI.

More elaborate methods implement the Fourier (spectral) transform to extract the carrier frequency (inversely proportional to the distance between LSP extrema, discussed above). Min and Gomez[186] developed the fast-Fourier-transform (FFT) sizing of large particles and applied phase-spectrum corrections to improve accuracy. Berge et al.[187] measured 2D LSPs near side-scattering direction of levitated particles. Their 1D sections are processed with the FFT using the Hanning window. Later Steiner et al.[188] developed spectral sizing techniques for large particles ($50 < x < 500$), which 1D LSP is measured from 85° to 95°. Results of the spectral method for 50 μm glass spheres agreed well with that of a full LSP fit.

Godefroy and Adjouadi[189] measured 2D LSPs of spherical particles and tested two inversion methods to determine size: a 1D section is constructed and the average distance between peaks and valleys is calculated; a 2D FFT is performed, and the radius of the outer ring in the spectrum is determined. In diffraction imaging technique[100] the diffraction pattern (2D LSP) was processed by the short-time-Fourier-transform (STFT). The derived carrier frequency also linearly correlates with the size. Additionally, the identification of bispheres was demonstrated using the same algorithm.[109] Pan et al.[125] examined the autocorrelation function of a 2D LSP and derived the inverse linear dependence of the particle size on the peak positions, where the coefficient depends on the cell morphology. This peak positions are equivalent to the distances between extrema in the original LSP, since the Fourier spectra of the latter and of its autocorrelation are tightly related.

Ulanowski et al.[118] analyzed 2D LSPs, using an analogy with Fraunhofer diffraction, and proposed an estimation of the particle size from the speckle size. However, this approach is hampered by the presence of image boundaries and a beamstop, which introduces additional frequencies. Hence, the proposed method is sensitive to various distortions and requires a fine-tuning, although the latter is assisted by an empirical criterion of the analysis quality. Later Walters et al.[25] conducted extensive particle simulations of coarse-mode aerosols (modeled as an aggregate of spheres) and showed a linear relationship between the inverse speckle width and the aggregate size.

Hoshino and Itoh[179] used the FFT sizing in the framework of Fraunhofer diffraction and combined it with measurements for multiple incident directions (similar to the methods in Section 4.2) for a shape classification and better sizing accuracy.

Semyanov et al.[190] applied the windowed FFT to 1D LSPs, measured with the SFC, to estimate the carrier frequency. It leads to the robust sizing of spheres in a wide range of RI and produces satisfactory estimates of the largest dimension of various non-spherical particles.[191–194] Later Romanov et al.[195] generalized this approach using additional spectral parameter (zero-frequency amplitude). The resulting 2D mapping was

inverted with interpolation, leading to fast and robust estimation of the size and RI of spheres in a limited range of RI. Further consideration of the phase spectrum allowed a sensitive non-sphericity estimation for near-spherical particles.[23] Konokhova et al.[90] proposed another spectral parameter, which extended the applicability domain of the spectral sizing.

To conclude this subsection, the low-dimension inversion using discrete signals is currently the most widely used method in commercial instruments for single-particle characterization. Possessing such advantages as speed and stability, they are severely limited in the models and applicability domains, which largely hampers their further development. The spectral methods, while retaining all these advantages, have potential for further development due to the larger information content of the underlying signals. Thus, a wide variety of spectral parameters can be devised (for the same experimental set-up) or the result of a spectral method can be used as a first step of a more elaborate inversion.

4.1.2. Nonlinear Regression

Since the appearance of angle-resolved measurements for single particles, which are naturally more sensitive to particle characteristics, the characterization methods based on a nonlinear regression (or fitting the theory to the experiment) have been gradually spreading. Their main part is a variation of particle characteristics until a satisfactory agreement between an experimental signal and a simulation is obtained. To quantify this agreement a cost function is used and, mathematically speaking, its global minimum is searched for. On the one hand, this approach employs all the information contained in a continuous signal and allows one to evaluate uncertainties of retrieved particle characteristics. On the other hand, it requires significant computational resources for each processed particle and rarely guarantees either uniqueness or robustness in advance, in contrast to low-dimensional inversion.

Already in 1998 Zakovic et al.[196] showed that even for homogeneous spheres the regression is non-trivial due to the complex dependence of an oscillating LSP on both the size and RI. Although satisfactory results are obtained for spheres in practice, more complex models run the risk of not having a unique solution, even in theory, that is, two sets of particle characteristics may have the same signal. While the latter possibility is negligible for sufficiently rich signals ($n \gg p$), related to it is the ubiquitous multiplicity of solutions for noisy experimental signals. More specifically, even for spheres there are multiple local minima with similar values of the cost function, which hampers efficient finding of the global minima and increases retrieval uncertainties.[46,197] For certain levels of noise this may even lead to a completely erroneous solution.[198]

Partly, this is caused by the universal use of the sum-of-squares (L^2-norm) cost function, which is convenient for statistical considerations (including estimation of uncertainties), but does not necessarily correspond to experimental or model errors (distortions) or to the subjective merit of the visual agreement between two oscillating functions. To address the latter issue Bartholomew-Biggs et al.[199] introduced an additional penalty term, based on the difference of the intensity-peak locations, into the cost function to exclude undesirable local minima. Similar idea was used in ref. [200] where the penalty term contained the difference of the main (carrier) Fourier frequencies, responsible for reproducing the distance between extrema of the experimental signal.

Another problem of regression is a high computational cost of global optimization, which increase exponentially with increasing p. Overall, there are two existing strategies: the solution of the direct problem in real time, that is, during the numerical optimization, or using a preliminary calculated dataset, which is further used for the nearest-neighbor interpolation (similar to a lookup database). Real-time light-scattering simulations are definitely more convenient for global optimization and any algorithm can be used for the latter, leading to a more robust and accurate solution. However, it is routinely feasible only if using the LM theory or some approximations. Any rigorous simulation method for non-spherical particles is orders of magnitude slower, severely limiting its applications. Notable examples include characterization of bispheres from a 1D LSP[201] and several applications of holography, discussed below. All other regression methods to characterize non-spherical particles (in large numbers) employ precomputed datasets.

Another issue is the choice of the initial guess, which can accelerate global optimization and is critical for local-optimization algorithms. This is commonly solved based on the prior information, but sometimes using another (approximate) characterization method, for instance, a spectral sizing,[202] the fitting by a simpler model (sphere),[53] the nearest-neighbor interpolation using a small dataset,[203] or image processing tools.[137] Let us further take a closer look at various examples of regression techniques.

Caramanica[204] used the particle-swarm optimization (PSO), a global optimization technique, for RBC characterization ($p = 4$) based on the synthetic measurement of a 1D LSP in the whole range of scattering angles. RBC parameters are then recovered within 1–4% using 1200 DDA evaluations. Charnigo et al.[205] provides a general discussion of regression, especially of the Bayesian approaches to estimating credible (confidence) intervals of retrieved particle characteristics. However, the critical issue of estimating the experimental noise (or choosing a model for it) is addressed only through auxiliary experiments, which is rigorous but not always feasible. Possibility of estimating the noise level from the discrepancy of the particular measurement is not discussed. Blohm et al.[206] retrieved two characteristics of a thin cylinder by fitting a 1D LSP with simulations based on the Fresnel–Kirchhoff diffraction.

Digital holography provides a lot of experimental information, given by rigorous Equation (8), but at the same time leads to larger p, since in addition to the inherent particle characteristics one has to also retrieve its orientation, position in space, and a normalization coefficient for the scattering intensity. The simplest case of a homogeneous sphere already leads to $p = 6$,[52] which makes even the LM theory insufficiently fast, justifying its GPU-acceleration.[137] Still, the robustness and speed of this approach largely depends on a good initial guess. Thus, the authors used the circular Hough transform[207] of a given hologram to obtain the in-plane position and the low-resolution Monte Carlo fitting for the size, RI, and axial position. Generally speaking, this method recognizes that some characteristics have relatively simple (smooth) influence on the experimental signal. The typ-

ical characterization result is 1.46 ± 0.02 μm and 1.55 ± 0.03 for the size and RI of a sphere, respectively. But it is not clear, whether the uncertainties correspond to 1 or 2 standard deviations (SD). This is a common shortcoming of many papers, which do not pay sufficient attention to the uncertainty estimation, only showing some standard values produced by the fitting routines. Unfortunately, evaluating uncertainties due to the experimental noise is much less trivial than calculating the real errors when using synthetic data. Therefore, while we quote several results for experimental characterization of spheres in this chapter, comparing uncertainties between different methods should be made with caution. Moreover, we do not discuss potential systematic biases.

Hannel et al.[208] showed that this characterization approach is relatively robust with respect to shape imperfections. Careful analysis of different types of errors was performed in various scenarios: a single measurement, repeated measurements in an optical trap, and when the particle freely diffuses in the measurement volume. Similarly, Wang et al.[145] characterized the dimension of fractal aggregates using the effective size and RI obtained from the LM characterization.

Further ingenious enhancement of holography characterization was performed by Dimiduk and Manoharan[140] using the Bayesian inference, which results in well-defined uncertainties of particle characteristics. For the global optimization in the case of spheres with $p = 6$ they employed the Markov-chain Monte Carlo (MCMC) algorithm and processed images for multiple particle positions using the constancy of size and RI. Thus, the posterior probability for one position is used as a prior to the next one, resulting in very small final uncertainties. For instance, the size and RI of a silica bead at 660 nm were determined as 961.6 ± 0.2 nm and 1.4898 ± 0.0002 (1 SD), respectively. In order to accelerate the direct problem, a small random subset of the hologram is used for fitting as described in ref. [139].

This approach was extended to non-spherical particles in refs. [53,141] where $p = 9$ and 10 for spherocylinders (capsules) and asymmetrically coated spheres, respectively. Moreover, the DDA was used for simulations, additionally contributing to enormous computational costs. To keep the latter manageable, the algorithm first quickly estimates characteristics (the position from the LM-theory fit, the orientation using a precomputed rotational dataset, the geometry from the scanning electron microscopy, and the RI from the bulk values) before performing the main fit with Levenberg–Marquardt algorithm (local optimization). During the latter the particle characteristics are assumed the same for all frames along the particle trajectory.

Probably, the largest p was obtained in the characterization of aggregates of spheres[142] with $p = 10$ for rigid clusters of six spheres and $p = 21$ for six small spheres on top of a larger one. The authors used, respectively, the MSTM and a superposition of independent LM solutions for simulations, assuming the same characteristics of spheres inside an aggregate. The number of spheres in a specific aggregate was determined prior to the fit using the Rayleigh–Sommerfeld reconstruction[209] (see also Section 4.2). The remaining fit residuals were larger than the expected noise level, indicating potential for further improvement using more sophisticated models (with even larger p).

Cheong et al.[210] showed that holography characterization can be applied in a turbid medium as well. Generally, turbidity decreases a signal-to-noise ratio and introduces certain biases, but comparable accuracy and precision can still be reached.

Strokotov et al.[47] formalized a complete description of the Bayesian approach to solve the parametric ILSP for 1D LSPs of coated spheres ($p = 4$) measured with the SFC. The DiRect algorithm[211] was used for the global minimization of a weighted sum of squared residuals. It provides an approximate description of these cost function over the whole range of particle characteristics as a byproduct, which is further transformed into the posterior probability density. The latter describes both uncertainties and confidence ranges/intervals of retrieved characteristics. The authors have recognized that both instrumental distortions (due to the complicated measurement of the LSP) and model errors (always present for biological cells) are far from the standard white-noise assumption. In particular, there is a significant correlation between residuals for nearby scattering angles. To address this issue, the cost function was assumed to belong to the χ^2 distribution (as for the white noise), but with a smaller number of degrees of freedom (n_{eff} instead of n). The latter can be estimated from the best-fit residual for a given particle through the sample autocorrelation function. Although this approach is empirical, it has some theoretical justification[212,213] and can be applied in almost any case, where the complete description of instrumental and/or model errors is not feasible.

The same characterization method was used for blood microparticles (extracellular vesicles),[11] also combining the standard LSP measurement with side- and forward-scattering signals.[93,214,215] Resulting characterization uncertainties significantly vary over the sample. The median size uncertainties (1 SD) were 8, 19, and 5 nm for 0.4 and 1 μm beads and near-spherical blood microparticles larger than 0.4 μm, respectively.[214] Corresponding median uncertainties of the RI were 0.002, 0.005, and 0.003, respectively. For near-spherical milk-fat globules (mostly from 0.5 to 4 μm) the median uncertainty (1 SD) of the size and RI were 74 nm and 0.009, respectively,[200] while the minimum uncertainties were 10 nm and 0.0015, respectively.[195]

While uncertainties or confidence regions of characteristics are insightful for characterization of a single particle (as in some holography examples above), it may cause information overload for flow systems, where thousands of particles are analyzed in each sample. Thus, in most cases the determined uncertainties are further ignored, except for average or median values to quantify overall characterization accuracy or for discarding a part of the sample (see below). In this case only distributions of the whole sample over characteristics are shown as the final results, using either best-fit values or mathematical expectations for each particle. Two notable exceptions are the following. Strokotov et al.[47] combined individual uncertainties to better estimate the distribution of a sample over characteristics, but they assumed that these distributions (as well as posterior distributions for individual particles) are multi-dimensional normal ones. Konokhova et al.[11] relaxed this assumption at the cost of neglecting correlations between different characteristics. They used a 1D deconvolution algorithm to estimate the sample distribution over each characteristic from a set of measurements with different uncertainties, assuming only that this distribution is sufficiently smooth.

For analysis of non-spherical particles with the SFC, using precomputed datasets is the only feasible option (with the only

exception of ref. [201]), since the DDA or T-matrix methods are used for light-scattering simulations. First attempts with small datasets were made by Yurkin et al.[216] and Kolesnikova et al.[217] for RBCs and blood platelets, respectively. Moskalensky et al.[48] presented a complete description of a discrete (dataset-based) Bayesian approach to solve a parametric ILSP. The method uses nearest-neighbor interpolation with estimates of uncertainties similar to the abovementioned DiRect-based method (including the use of n_{eff}). The only difference is that the cost-function evaluations during the DiRect run (with values of characteristics denser placed near the solution) are replaced by values of the cost function for a dataset uniformly distributed in the space of characteristics. The corresponding errors can be analyzed by Monte-Carlo-based formulas, and are negligible for sufficiently large datasets (and moderate p). Moreover, the dependence of the minimum value of the cost function, averaged over the sample, on the dataset size can be used to judge the sufficiency of the latter.

Originally, the dataset-based method was applied to blood platelets (oblate spheroids),[48,218] *E. coli* bacteria (capsules),[64] and microparticle aggregates (bispheres)[214] with $p = 4$, as well as for RBCs (biconcave discoids) with $p = 5$.[91,219] In the case of bacteria the confidence region of retrieved characteristics was used for quality control.[64] For part of the cells this region consisted of two distant domains in coordinates of the length versus the diameter or orientation angle, hence, the region width was compared against a threshold to discard a part of the sample. Similar issue has been studied for oblate spheroids,[48] where the low sensitivity of the 1D LSP to simultaneous change of the size, aspect ratio, and RI was explained in the framework of the AD approximation.

The developed algorithms have also been used for assessing the adequacy of shape models. The simplest qualitative approach is testing an alternative model and comparing the corresponding changes in the LSP with the typical fit residuals.[64,216,217] Another option is to feed the simulated signal for an alternative model into the regression method and test whether the obtained confidence ranges of characteristics are consistent with the true values.[47] Such comparison also tests the robustness of the uncertainties estimation with respect to model errors. Similarly, obtained uncertainties (or other quality-of-fit parameters) has been used to discard a part of the processed particles, as belonging to an alternative (more complicated) model.[11,64,215] Finally, the most rigorous approach is to try a regression with different models and choose the most suitable one for a specific particle. Examples include using the F-test and the Bayesian information criterion for nested (spheres and spheroids[200]) and non-nested models (spheres and bispheres[93,214]), respectively.

Large computational costs are highlighted throughout this section. Two obvious acceleration options are using the computing cluster and/or GPUs. The latter was discussed in detail by Jakubczyk et al.[66] for LM fits to the measured LSPs, using the CUDA platform. Later Derkachov et al.[220] improved the system with the image-formation (raytracing) subroutines, that is, relating the LM angle-resolved scattering with the actual CCD image. Dataset-based characterization is relatively fast (on the order of 1 s per particle, not accounting for building the dataset itself), but even this can be insufficient for high-throughput applications. Muliukov and Yurkin[221] proposed acceleration based on preliminary clustering of the dataset, leading to more than ten times acceleration.

To conclude, nonlinear regression is currently the most advanced approach, leading to robust results, including the retrieval uncertainty for a single particle. It is compatible with high-throughput systems and can be straightforwardly applied for any parametric shape model with several parameters. Spherical micron-sized particles can be routinely characterized with size uncertainties about 10 nm and in some cases as small as 1 nm. Uncertainties of RI are from 0.01 to less than 0.001. For non-spherical particles uncertainties are generally larger, but in many cases they are still much smaller than the diffraction limit of standard microscopy. However, this approach has a very high computational cost related to the global optimization, which becomes prohibitive with the increasing number of model parameters. Moreover, it requires a separate consideration of the model adequacy for a particular application. Promising directions for further research include an optimization of computational algorithms for more complex shape models, better understanding of experimental distortions for a more reliable uncertainty estimation, and a combination of characterization results from different particles in a sample or from different measurements of the same particle.

4.1.3. Neural Network Approach

In many ways this approach resembles low-dimensional inversion (see Section 4.1.1), only here the signal parameters are not designed manually but are formed automatically inside a "black box." Advantages of this approach are high execution speed and potential direct applicability to any measurement system. However, this comes at expense of required fine-tuning and poor predictability of the robustness and accuracy of the final result.

The first attempt to characterize spheres with a NN was made by Ulanowski et al.[222] in 1998. They trained a radial-basis-function (RBF) NN with one hidden layer assuming the noise-free measurement of a full-range 1D LSP. They obtained the maximum and mean relative errors of the order of 10^{-3} and 10^{-5}, respectively, and showed that two thirds of the whole LSP can be removed without significant loss in accuracy. Later Wang et al.[223] used a sequence of two RBF NNs, which operate on global and local scales in the space of characteristics. Absorbing spheres were considered in ref. [224] and showed promising results in the presence of synthetic noise. However, the LSP was again assumed to be measured in the whole range of angles, which is not realistic.

The latter limitation was removed by Berdnik et al.[225] They constructed a high-order NN to characterize spheres with weak absorption from the LSPs in the range from 10° to 60°. Polynomial approximations and the Fourier spectrum of the LSP were used to compose the input signal vector, which is an illustrative example of manual fine-tuning. Moreover, a single dense layer was used in combination with a signal spreader, which divides the components of an input signal into several groups—each is transferred to a specific neuron. Based on testing with a synthetic noise the standard retrieval errors were 0.08, 0.012 and 0.18, 0.017, 0.003 for the size, the real and imaginary parts of RI in the non-absorbing and absorbing cases, respectively. This NN was, for the first time, tested on real experimental data from

the SFC, showing similar spread of results. However, the retrieval of the RI was significantly less accurate than that using the nonlinear regression. Later, the network architecture was changed to three fully connected layers and the range of characteristics was increased, resulting in similar retrieval errors.[226] More detailed information is provided in ref. [227].

Recently, the same approach has been extended to particles in air (aerosols)[228] using a three-layers perceptron NN with a hyperbolic-tangent activation function. To obtain a robust performance, a polychromatic (white-light) illumination is considered, and the LSP is integrated over several collection angles (intervals). While the results were reasonably insensitive to a synthetic noise, no real experiments were considered.

Concerning non-spherical particles, Berdnik et al.[229,230] applied NNs to optically soft spheroids using the RGD approximation for simulation of 2D LSPs. They used a linear activation function in a three-level RBF NN, in which each level was trained on a specific subrange of the size parameter relative to the previous level. Only a synthetic experimental noise was considered. Apostolopoulos et al.[114] performed an extensive theoretical study to develop an identification and characterization method of RBCs from multi-spectral (white-light) scattering images (SALS captured by a standard CCD matrix). The ILSP is solved by RBF NNs, which operate on features extracted from images by the angular radial transform, the Zernike transform, and the Gabor filters bank. Only a synthetic experimental noise has been considered, but it also included possible distortions due to the imperfect alignment of the optical system.

On the one hand, NNs has not yet demonstrated any impressive results in real experiments. On the other hand, based on the architecture of the used NNs it seems that the potential of this approach is far from being fully exploited. The researchers mostly implemented simple multilayer perceptron-like NNs and has never used convolution layers. Moreover, the focus was shifted to the manual design of signal preprocessing, which contradicts the much desired black-box (automatic-learning) approach in NN applications. Recently, more complex NN architectures have been applied to classification light-scattering problems (see Section 4.3), which makes it promising for characterization problems as well.

4.2. Reconstruction

Unlike the previous methods to solve the ILSP, this approach does not require a particle model, but rather reconstructs the whole distribution of the RI in space—a function $m(\mathbf{r})$. This is also known as a coefficient inverse problem, if differential Maxwell's equations are considered as a forward model.[231] The necessary prior information is reflected mostly in the approximation used or in the knowledge of the RI value (then only the boundary is reconstructed). The main drawback of these methods is the enormous amount of required experimental data, severely limiting high-throughput implementations.

In general, such methods are common in holographic conditions; they are based on the scalar-diffraction approximation and deserve a separate review.[42] As explained in Chapter 2, they approximately retrieve $t(x, y)$ (an image), instead of fitting rigorous Equation (8). For example, the Fresnel–Kirchhoff approximation[42] was used for holographic reconstructions of large aerosol particles.[147,148,232] If the particle size is changing in time, the double-exposure hologram can also be used for the reconstruction leading to an image, where both sizes are clearly visible.[233]

More recently Carpio et al.[234,235] developed another holographic reconstruction algorithm based on the topological derivatives of the electromagnetic field. First, they used a scalar forward model and assumed the RI close to 1 to build a two-step algorithm, which determines support of the scatterer (where the RI is different from 1), and then fits the RI using a spherical approximation to the particle or its components.[234] Next, they improved the algorithm for 3D shape reconstruction, using the topological and Frechet (shape) derivatives of the cost (residual) functional based on holography measurements.[235] This algorithm can determine both the number of components and the shape of each one, assuming that the RI is constant and known. Moreover, it describes, how any light-scattering method can be adapted to calculate corresponding derivatives, by using a specially formed incident field. Thus, the shape fitting can potentially be used with other measurement systems as well.

Generally, the specific quantitative capabilities (accuracy) of holographic reconstruction is not completely clear. Both complex numerical approaches[234,235] and straightforward Fourier-like transformations lead to visually comparable results. For example, the shape of a 1 μm trapped aerosol particle was obtained using the Kirchhoff–Helmholtz transform.[236] Nevertheless, such a technique may simplify a solution of the ILSP providing a starting point for regression methods.

Another approach is based on the standard scattering measurement (discretized 2D LSP) but for many incident directions, similar to that used in the tomography. However, the principal difference of the latter (in application to single particles) is that it assumes some approximation, which makes the scattered electric fields linear in the function $m(\mathbf{r})$, similar to the holography above. For example, the X-ray tomography takes into account only attenuation and phase shift, while diffraction tomography additionally assumes weak scattering (using the RGD or Rytov approximations).[41] Typically only the intensity is measured, but under the above approximations the phase can be retrieved as well.[237,238] By contrast, Chaumet et al.[239–241] used no approximations, solving the direct problem with the DDA. The particle is discretized into voxels, which RIs are treated as variables, and the reconstruction is based on the inversion of the DDA numerical scheme. In some sense, it is similar to the model-based methods (Section 4.1.2), but with a few thousand characteristics. The major limitation, however, is that these methods have been tested only on synthetic data assuming that the field phase is available.

Finally, we briefly mention the characterization techniques developed for the microwave scattering instruments.[69] While the electromagnetic scale invariance rule[35] implies equivalence of the corresponding problem to that of light-scattering one, the main (technical) advantage of microwaves is a direct measurement of the field phase and better independent control of particle morphology (which are mm to cm in size). On the one hand, this enabled application of voxel-based reconstruction techniques discussed above.[70,242] On the other hand, various advanced methods have also been applied, such as the linear sampling method,[243,244] the contrast source inversion

method,[245,246] and the factorization method.[247,248] However, it is still unclear whether these methods can be applied at optical frequencies, although the interference-based measurement of field phases is possible.[249,250]

While reconstruction techniques are surely promising and will benefit from further instrumental development, their specific applicability for accurate characterization (rather than imaging) remains questionable. Most of the described algorithms, which are based on the rigorous light-scattering theory, are still only proofs of principle.

4.3. Data-Driven

In contrast to the model-driven approach, here the prior information is the collected data itself, the model is not considered at all, and the characterization problem is reduced to the identification or classification. It is hard to describe these methods in general, since the presented results mostly demonstrate the possibility of classification for a specific practical implementation. The main focus here is on the construction of features (signal parameters), which generally determines the success in machine learning algorithms (similar to the conclusion of Section 4.1.3).

Already in 1992 Bevan et al.[251] made a particle classifier based on an NN (a multi-layer perceptron) using three side-scattering signals and a forward-scattering one (as in ref. [78]). Later Boddy et al.[252] used a one-layer RBF NN for phytoplankton identification using seven signals, but only two of them were light-scattering ones. Morris et al.[253] showed that the support-vector machine (SVM) algorithm leads to better results. Rajwa et al.[63] used the SVM algorithm trained on experimental data to distinguish four types of cells using four signals, which were selected based on the DDA simulations using the cell shape models (hence, the approach is not completely model-free).

The classification of six types of different cells was performed using diffraction images (2D LSPs) and an SVM-based algorithm with features obtained from the image analysis algorithm, called the gray level co-occurrence matrix (GLCM).[50] Accuracy for classification into two broad groups (white-blood-cells derived and epithelial derived cells), each comprising three cell types, was 94%, however it can be as low as 54% for classification into six types. This system was further improved to acquire two cross-polarized diffraction images.[96,104,105] The authors divided images into three classes by their speckle patterns which are associated with the order of size and morphological heterogeneity. With this system it was possible to reliably distinguish quite similar in morphology Jurkat T and Ramos B cells at 98% accuracy.[106,108] Classification into spheres, cylinders, and ellipsoids with different RIs has been performed using unsupervised machine learning based on the Gaussian mixture model and features obtained from the GLCM.[51] The authors found that GLCM parameters combined with the integrated forward scattering intensity are sufficient to achieve 98% accuracy of the classification. Later Zhang et al. compared the contourlet transform with the GLCM—the latter showed better results.[254] Recently Xie et al.[107] used the gray-level differential statistics and the SVM with leave-one-out cross-validation to identification of the acute and chronic myeloid leukemic cells, achieving sensitivity of 92% and a specificity of 95%.

Crosta et al.[126] performed an automatic classification of several classes of airborne particles, including bacteria, based on measured 2D LSPs. The latter is first transformed into a number of features, including those based on the Fourier transform of the image. A lot of different versions of the classifier based on the principal-component analysis (PCA), using the supervised training on real data, were tested with overall satisfactory results. Later Holler et al.[110] used LSPs measured at two wavelengths to classify biological aerosols. The mean intensity, results of the Watershed processing, the image entropy, and a modified autocorrelation were used as features in the discriminant-function analysis and the PCA.

The SALS signals were used by Grant-Jacob et al.[255] to determine the number of scattering particles and their material with the use of an NN trained on microscopic data of the same sample. The NN consisted of two convolutional layers with a fully connected layer (1024 neurons). Later Su et al.[256] classified cancer cells with the use of the SVM and features obtained from the histograms of oriented gradients applied to a 2D LSP. Recently Ding[257] demonstrated a potential of convolutional NNs to classify particles shape by a 2D LSP with accuracy above 97%.

To conclude, the field of light-scattering classification and identification using instruments with discrete or continuous signals is relatively mature. Recent accuracy of classification is well above 90%, using various techniques to extract features. However, the latter hampers automatic application of this approach, since competent choice of features is largely a manual and empiric procedure. Judging by the trends and enormous success of deep learning in multitude of other fields, a further promising direction of research in light-scattering classification is using well-built NN architecture that would take original signals as input without a preliminary computation of any features.

5. Conclusion

We have reviewed various ELS methods for single particle characterization. In the instrumental part, we have highlighted two main aspects—particle isolation and measurement, discussing both the historical development and the state of the art. Although most commercial characterization instruments still use only several discrete signals, the angle-resolved measurements (1D and 2D LSPs) are quickly catching up and have already demonstrated unprecedented capabilities in various applications. These capabilities are enabled by characterization (data-processing) algorithms, which are discussed in details in the main part of the review.

We have classified the existing approaches depending on the provided prior information. Most developments belong to the class of the model-driven methods, based on the solution of parametric inverse light-scattering problems, typically performed by a nonlinear regression. The best results so far were demonstrated by the scanning flow cytometry and digital holography, which provide reliable characterization of both spherical and non-spherical particles with accuracy much better than the diffraction limit. The state-of-the-art approach for the latter is to accelerate a nonlinear regression using preliminary computed datasets. Unfortunately, little attention is paid to the important issue of characterization uncertainties. This relates both to the uncertainties themselves, without which the obtained

characteristics cannot be used in any quantitative manner, and the methods of estimating them, especially in the presence of both model and instrumental distortions. A related promising research direction is combining many individual characterizations, either of the same particle (e.g., in holography) or of the same-type particles (in high-throughput systems).

We have also considered the methods based on a low-dimensional inversion. When applied to discrete-signal instruments, they have mostly exhausted their potential. However, they are definitely promising in combination with continuous signals (which are compressed into a few parameters). The prominent example is the spectral methods that are widely used for rapid sizing but lack a rigorous theoretical foundation for further development. There were also some developments based on the neural networks (machine learning). While the existing results are far from impressive, there is a clear potential for using modern complex network architectures and training techniques (deep learning) for both classification and characterization.

Reconstruction methods requiring no prior particle model deserve a special mention. When linearizing approximations are assumed, such methods are widely used in the framework of either holography or tomography. But those methods are semi-quantitative imaging ones, which leaves them outside of the scope of this review. Otherwise, certain progress has been demonstrated in microwave-scattering experiments with straightforward phase measurements. But the most interesting problem of approximation-free reconstruction of a single particle from the optical measurements remains largely open with only a few proofs of principle demonstrating limited success. This problem is definitely a holy grail of the single-particle characterization and a prerequisite for handling truly unknown samples.

To conclude, ELS single-particle characterization is currently a mature field with many real-life applications. Several existing methods has already demonstrated impressive results and have a large potential for further development due to improving instrumental and computational capabilities. But even more promising is a combination of various methods and ideas, such as using a spectral method or an approximate reconstruction to provide a starting point for nonlinear-regression methods. Hopefully, this review will facilitate such synergistic development.

Acknowledgements

The work was supported by the Russian Foundation for Basic Research (grant No. 19-32-90073). The authors thank two anonymous reviewers for their constructive comments.

Conflict of Interest

The authors declare no conflict of interest.

Keywords

characterization, elastic light scattering, inverse problem, machine learning, optimization, single particle

Received: August 27, 2020
Revised: November 17, 2020
Published online: January 15, 2021

[1] M. Schnaiter, O. Schmid, A. Petzold, L. Fritzsche, K. F. Klein, M. O. Andreae, G. Helas, A. Thielmann, M. Gimmler, O. Möhler, C. Linke, U. Schurath, *Aerosol Sci. Technol.* **2005**, *39*, 249.
[2] R. Vehring, C. L. Aardahl, G. Schweiger, E. J. Davis, *J. Aerosol Sci.* **1998**, *29*, 1045.
[3] S. Schutzmann, I. Venditti, P. Prosposito, M. Casalboni, M. V. Russo, *Opt. Express* **2008**, *16*, 897.
[4] C. Bohren, D. Huffman, *Absorption and Scattering of Light by Small Particles*, Wiley, New York **1983**.
[5] M. I. Mishchenko, L. D. Travis, A. A. Lacis, *Scattering, Absorption, and Emission of Light by Small Particles*, Cambridge University Press, Cambridge **2002**.
[6] M. Kerker, M. I. Hampton, *J. Opt. Soc. Am.* **1953**, *43*, 370.
[7] D. L. Jaggard, C. Hill, R. W. Shorthill, D. Stuart, M. Glantz, F. Rosswog, B. Taggart, S. Hammond, *Atmos. Environ.* **1981**, *15*, 2511.
[8] C. O. R. Abbireddy, C. R. I. Clayton, *Proc. Inst. Civil Eng. Geotech. Eng.* **2009**, *162*, 193.
[9] J. Stetefeld, S. A. McKenna, T. R. Patel, *Biophys. Rev.* **2016**, *8*, 409.
[10] T. Sanvito, P. Bigini, M. V. Cavanna, F. Fiordaliso, M. B. Violatto, L. Talamini, M. Salmona, P. Milani, M. A. C. Potenza, *Nanomedicine* **2017**, *13*, 2597.
[11] A. I. Konokhova, M. A. Yurkin, A. E. Moskalensky, A. V. Chernyshev, G. A. Tsvetovskaya, E. D. Chikova, V. P. Maltsev, *J. Biomed. Opt.* **2012**, *17*, 057006.
[12] A. E. Bulyshev, A. E. Souvorov, S. Y. Semenov, V. G. Posukh, Y. E. Sizov, *Inverse Probl.* **2004**, *20*, 1239.
[13] F. J. G. de Abajo, *Rev. Mod. Phys.* **2010**, *82*, 209.
[14] C. Cherqui, N. Thakkar, G. Li, J. P. Camden, D. Masiello, *Annu. Rev. Phys. Chem.* **2016**, *67*, 331.
[15] T. Coenen, E. J. R. Vesseur, A. Polman, *Appl. Phys. Lett.* **2011**, *99*, 143103.
[16] R. W. Applegate, D. N. Schafer, W. Amir, J. Squier, T. Vestad, J. Oakey, D. W. M. Marr, *J. Opt. A: Pure Appl. Opt.* **2007**, *9*, S122.
[17] E. van der Pol, F. A. W. Coumans, A. Sturk, R. Nieuwland, T. G. van Leeuwen, *Nano Lett.* **2014**, *11*, 6195.
[18] N. Mohandas, Y. R. Kim, D. H. Tycko, J. Orlik, J. Wyatt, W. Groner, *Blood* **1986**, *68*, 506.
[19] P. A. Lane, M. B. Hart, V. Jain, J. E. Tucker, J. D. Eversole, *J. Quant. Spectrosc. Radiat. Transfer* **2018**, *208*, 188.
[20] N. Moteki, *J. Quant. Spectrosc. Radiat. Transfer* **2020**, *243*, 106811.
[21] E. J. Davis, E. Chorbajian, *Ind. Eng. Chem. Fundam.* **1974**, *13*, 272.
[22] L. Zhang, X. Chen, Z. Zhang, W. Chen, H. Zhao, X. Zhao, K. Li, L. Yuan, *Rev. Sci. Instrum.* **2016**, *87*, 044301.
[23] A. V. Romanov, A. I. Konokhova, E. S. Yastrebova, K. V. Gilev, D. I. Strokotov, V. P. Maltsev, M. A. Yurkin, *J. Quant. Spectrosc. Radiat. Transfer* **2019**, *235*, 317.
[24] S. Holler, Y. Pan, R. K. Chang, J. R. Bottiger, S. C. Hill, D. B. Hillis, *Opt. Lett.* **1998**, *23*, 1489.
[25] S. Walters, J. Zallie, G. Seymour, Y.-L. Pan, G. Videen, K. B. Aptowicz, *J. Quant. Spectrosc. Radiat. Transfer* **2019**, *224*, 439.
[26] J. Garcia-Sucerquia, W. Xu, S. K. Jericho, P. Klages, M. H. Jericho, H. J. Kreuzer, *Appl. Opt.* **2006**, *45*, 836.
[27] A. R. Glover, S. M. Skippon, R. D. Boyle, *Appl. Opt.* **1995**, *34*, 8409.
[28] L. Vásárhelyi, Z. Kónya, Á. Kukovecz, R. Vajtai, *Mater. Today Adv.* **2020**, *8*, 100084.
[29] M. Kinnunen, A. Karmenyan, *J. Biomed. Opt.* **2015**, *20*, 051040.
[30] J. R. Frisvad, H. Kragh, *Eur. Phys. J. H* **2019**, *44*, 137.
[31] M. I. Mishchenko, L. D. Travis, *J. Quant. Spectrosc. Radiat. Transfer* **1998**, *60*, 309.
[32] A. Taflove, S. C. Hagness, *Advances in Computational Electrodynamics: The Finite-Difference Time-Domain Method*, 3rd ed., Artech House, Boston **2005**.

[33] M. A. Yurkin, A. G. Hoekstra, *J. Quant. Spectrosc. Radiat. Transfer* **2007**, *106*, 558.
[34] M. Kahnert, *J. Quant. Spectrosc. Radiat. Transfer* **2016**, *178*, 22.
[35] M. I. Mishchenko, *Electromagnetic Scattering by Particles and Particle Groups: An Introduction*, Cambridge University Press, Cambridge **2014**.
[36] J. Lim, H. Ding, M. Mir, R. Zhu, K. Tangella, G. Popescu, *Biomed. Opt. Express* **2011**, *2*, 2784.
[37] Y. Sung, G. Barbastathis, *Opt. Express* **2013**, *21*, 2674.
[38] S. Assili, *ArXiv:1808.09172 [Physics]*, **2018**.
[39] *Optical Coherence Tomography: Technology and Applications*, 2nd ed. (Eds: W. Drexler, J. G. Fujimoto), Springer International Publishing, New York **2015**.
[40] L. W. Goldman, *J. Nucl. Med. Technol.* **2007**, *35*, 115.
[41] P. Müller, M. Schürmann, J. Guck, *ArXiv:1507.00466 [Physics, q-Bio]*, **2016**.
[42] M. K. Kim, *J. Photonics Energy* **2010**, *1*, 018005.
[43] T. Tahara, X. Quan, R. Otani, Y. Takaki, O. Matoba, *Microscopy* **2018**, *67*, 55.
[44] N. Chen, S. Rehman, C. J. R. Sheppard, *Crit. Rev. Biomed. Eng.* **2013**, *41*, 393.
[45] J. D. Morris, C. K. Payne, *Annu. Rev. Phys. Chem.* **2019**, *70*, 199.
[46] V. P. Maltsev, K. A. Semyanov, *Characterisation of Bio-Particles from Light Scattering*, VSP, Utrecht **2004**.
[47] D. I. Strokotov, M. A. Yurkin, K. V. Gilev, D. R. van Bockstaele, A. G. Hoekstra, N. B. Rubtsov, V. P. Maltsev, *J. Biomed. Opt.* **2009**, *14*, 064036.
[48] A. E. Moskalensky, M. A. Yurkin, A. I. Konokhova, D. I. Strokotov, V. M. Nekrasov, A. V. Chernyshev, G. A. Tsvetovskaya, E. D. Chikova, V. P. Maltsev, *J. Biomed. Opt.* **2013**, *18*, 017001.
[49] Y.-L. Pan, K. B. Aptowicz, R. K. Chang, M. Hart, J. D. Eversole, *Opt. Lett.* **2003**, *28*, 589.
[50] K. Dong, Y. Feng, K. M. Jacobs, J. Q. Lu, R. S. Brock, L. V. Yang, F. E. Bertrand, M. A. Farwell, X. H. Hu, *Biomed. Opt. Express* **2011**, *2*, 1717.
[51] W. Wang, Y. Wen, J. Q. Lu, L. Zhao, S. A. Al-Qaysi, X.-H. Hu, *J. Quant. Spectrosc. Radiat. Transfer* **2019**, *224*, 453.
[52] S.-H. Lee, Y. Roichman, G.-R. Yi, S.-H. Kim, S.-M. Yang, A. van Blaaderen, P. van Oostrum, D. G. Grier, *Opt. Express* **2007**, *15*, 18275.
[53] A. Wang, T. G. Dimiduk, J. Fung, S. Razavi, I. Kretzschmar, K. Chaudhary, V. N. Manoharan, *J. Quant. Spectrosc. Radiat. Transfer* **2014**, *146*, 499.
[54] R. Alexander, B. Leahy, V. N. Manoharan, *J. Appl. Phys.* **2020**, *128*, 060902.
[55] H. C. van de Hulst, *Light Scattering by Small Particles*, Dover, New York **1981**.
[56] B. Gallinet, J. Butet, O. J. F. Martin, *Laser Photonics Rev.* **2015**, *9*, 577.
[57] T. Latychevskaia, H.-W. Fink, *Appl. Opt.* **2015**, *54*, 2424.
[58] J.-L. Castagner, I. J. Bigio, *Appl. Opt.* **2006**, *45*, 2232.
[59] C. Gardiner, M. Shaw, P. Hole, J. Smith, D. Tannetta, C. W. Redman, I. L. Sargent, *J. Extracell. Vesicles* **2014**, *3*, 25361.
[60] M. L. Shuler, R. Aris, H. M. Tsuchiya, *Appl. Microbiol.* **1972**, *24*, 384.
[61] J. F. D. L. Mora, P. Riesco-Chueca, *J. Fluid Mech.* **1988**, *195*, 1.
[62] C. Ba, W. J. Shain, T. G. Bifano, J. Mertz, *Biomed. Opt. Express* **2018**, *9*, 6145.
[63] B. Rajwa, M. Venkatapathi, K. Ragheb, P. P. Banada, E. D. Hirleman, T. Lary, J. P. Robinson, *Cytometry, Part A* **2008**, *73*, 369.
[64] A. I. Konokhova, A. A. Gelash, M. A. Yurkin, A. V. Chernyshev, V. P. Maltsev, *Cytometry, Part A* **2013**, *83*, 568.
[65] A. Bain, T. C. Preston, *J. Appl. Phys.* **2019**, *125*, 093101.
[66] D. Jakubczyk, S. Migacz, G. Derkachov, M. Woźniak, J. Archer, K. Kolwas, *Opto-Electron. Rev.* **2016**, *24*, 108.
[67] M. Kinnunen, J. Tuorila, T. Haapalainen, A. Karmenyan, V. Tuchin, R. Myllylä, *SPIE Proc.* **2014**, *9031*, 90310A.
[68] M. Kinnunen, A. Kauppila, A. Karmenyan, R. Myllylä, *Biomed. Opt. Express* **2011**, *2*, 1803.
[69] J. M. Geffrin, P. C. Chaumet, C. Eyraud, K. Belkebir, P. Sabouroux, *Appl. Phys. Lett.* **2008**, *92*, 194103.
[70] P. C. Chaumet, K. Belkebir, *Inverse Probl.* **2009**, *25*, 024003.
[71] R. M. P. Doornbos, M. Schaeffer, A. G. Hoekstra, P. M. A. Sloot, B. G. de Grooth, J. Greve, *Appl. Opt.* **1996**, *35*, 729.
[72] E. S. Cross, T. B. Onasch, M. Canagaratna, J. T. Jayne, J. Kimmel, D. R. Worsnop, P. Davidovits, *Atmos. Chem. Phys.* **2009**, *25*, 7769.
[73] R. J. Gill, S. Mohan, E. L. Dreizin, *Rev. Sci. Instrum.* **2009**, *80*, 064101.
[74] X. Wang, G. Chancellor, J. Evenstad, J. E. Farnsworth, A. Hase, G. M. Olson, A. Sreenath, J. K. Agarwal, *Aerosol Sci. Technol.* **2009**, *43*, 939.
[75] V. A. Loiko, G. I. Ruban, O. A. Gritsai, A. D. Gruzdev, S. M. Kosmacheva, N. V. Goncharova, A. A. Miskevich, *J. Quant. Spectrosc. Radiat. Transfer* **2006**, *102*, 73.
[76] D. H. Tycko, M. H. Metz, E. A. Epstein, A. Grinbaum, *Appl. Opt.* **1985**, *24*, 1355.
[77] R. A. Flynn, B. Shao, M. Chachisvilis, M. Ozkan, S. C. Esener, *Biomed. Microdevices* **2005**, *7*, 93.
[78] L. Ding, J. Zhang, H. Zheng, Y. Wang, L. Fang, *Atmos. Environ.* **2016**, *139*, 87.
[79] W. W. Szymanski, A. Nagy, A. Czitrovszky, P. Jani, *Meas. Sci. Technol.* **2002**, *13*, 303.
[80] H. Umhauer, M. Bottlinger, *Appl. Opt.* **1991**, *30*, 4980.
[81] S. G. Ackleson, R. W. Spinrad, *Appl. Opt.* **1988**, *27*, 1270.
[82] M. A. C. Potenza, T. Sanvito, A. Pullia, *J. Nanopart. Res.* **2015**, *17*, 110.
[83] M. Potenza, P. Milani, *J. Nanopart. Res.* **2014**, *16*, 1.
[84] A. K. Ray, A. Souyri, E. J. Davis, T. M. Allen, *Appl. Opt.* **1991**, *30*, 3974.
[85] M. Nakagawa, T. Nakayama, H. Sasago, S. Ueda, D. S. Venables, Y. Matsumi, *Aerosol Sci. Technol.* **2016**, *50*, 392.
[86] A. Abdelmonem, E. Järvinen, D. Duft, E. Hirst, S. Vogt, T. Leisner, M. Schnaiter, *Atmos. Meas. Tech.* **2016**, *9*, 3131.
[87] A. Abdelmonem, M. Schnaiter, P. Amsler, E. Hesse, J. Meyer, T. Leisner, *Atmos. Meas. Tech.* **2011**, *4*, 2125.
[88] M. Schnaiter, E. Järvinen, P. Vochezer, A. Abdelmonem, R. Wagner, O. Jourdan, G. Mioche, V. N. Shcherbakov, C. G. Schmitt, U. Tricoli, Z. Ulanowski, A. J. Heymsfield, *Atmos. Chem. Phys.* **2016**, *16*, 5091.
[89] V. P. Maltsev, *Rev. Sci. Instrum.* **2000**, *71*, 243.
[90] A. I. Konokhova, E. S. Yastrebova, D. I. Strokotov, A. V. Chernyshev, A. A. Karpenko, V. P. Maltsev, *J. Quant. Spectrosc. Radiat. Transfer* **2019**, *235*, 204.
[91] K. V. Gilev, E. S. Yastrebova, D. I. Strokotov, M. A. Yurkin, N. A. Karmadonova, A. V. Chernyshev, V. V. Lomivorotov, V. P. Maltsev, *Cytometry A* **2017**, *91*, 867.
[92] D. I. Strokotov, A. E. Moskalensky, V. M. Nekrasov, V. P. Maltsev, *Cytometry A* **2011**, *79A*, 570.
[93] A. I. Konokhova, D. N. Chernova, D. I. Strokotov, A. A. Karpenko, A. V. Chernyshev, V. P. Maltsev, M. A. Yurkin, *J. Biomed. Opt.* **2016**, *21*, 115003.
[94] G. V. Dyatlov, K. V. Gilev, K. A. Semyanov, V. P. Maltsev, *Meas. Sci. Technol.* **2008**, *19*, 015408.
[95] L. A. Philips, D. B. Ruffner, F. C. Cheong, J. M. Blusewicz, P. Kasimbeg, B. Waisi, J. R. McCutcheon, D. G. Grier, *Water Res.* **2017**, *122*, 431.
[96] H. Wang, Y. Feng, Y. Sa, J. Q. Lu, J. Ding, J. Zhang, X.-H. Hu, *Pattern Recognit.* **2017**, *61*, 234.
[97] D. Dannhauser, D. Rossi, P. Memmolo, F. Causa, A. Finizio, P. Ferraro, P. A. Netti, *J. Biophotonics* **2017**, *10*, 683.
[98] S. Wang, J. Liu, J. Q. Lu, W. Wang, S. A. Al-Qaysi, Y. Xu, W. Jiang, X. Hu, *J. Biophotonics* **2019**, *12*, e201800287.
[99] K. M. Jacobs, J. Q. Lu, X.-H. Hu, *Opt. Lett.* **2009**, *34*, 2985.

[100] S. Yu, J. Zhang, M. S. Moran, J. Q. Lu, Y. Feng, X.-H. Hu, *Opt. Express* **2012**, *20*, 22245.
[101] K. M. Jacobs, L. V. Yang, J. Ding, A. E. Ekpenyong, R. Castellone, J. Q. Lu, X.-H. Hu, *J. Biophotonics* **2009**, *2*, 521.
[102] X.-H. Hu, J. Q. Lu, in *Advanced Optical Flow Cytometry* (Ed: V. V. Tuchin), Wiley-VCH Verlag GmbH & Co. KGaA, Weinheim, Germany **2011**, pp. 311–331.
[103] Y. Sa, Y. Feng, K. M. Jacobs, J. Yang, R. Pan, I. Gkigkitzis, J. Q. Lu, X.-H. Hu, *Cytometry, Part A* **2013**, *83*, 1027.
[104] H. Wang, Y. Feng, Y. Sa, Y. Ma, J. Q. Lu, X.-H. Hu, *Appl. Opt.* **2015**, *54*, 5223.
[105] J. Zhang, Y. Feng, M. S. Moran, J. Q. Lu, L. V. Yang, Y. Sa, N. Zhang, L. Dong, X.-H. Hu, *Opt. Express* **2013**, *21*, 24819.
[106] Y. Feng, N. Zhang, K. M. Jacobs, W. Jiang, L. V. Yang, Z. Li, J. Zhang, J. Q. Lu, X.-H. Hu, *Cytometry* **2014**, *85*, 817.
[107] L. Xie, Q. Liu, C. Shao, X. Su, *Opt. Express* **2017**, *25*, 29365.
[108] N. Zhang, Y. Sa, Y. Guo, W. Lin, P. Wang, Y. Feng, *Curr. Bioinf.* **2018**, *13*, 50.
[109] W. Wang, J. Liu, J. Q. Lu, J. Ding, X.-H. Hu, *Opt. Express* **2017**, *25*, 9628.
[110] S. Holler, S. D. Fuerstenau, C. R. Skelsey, *J. Quant. Spectrosc. Radiat. Transfer* **2016**, *178*, 167.
[111] S. Holler, S. Zomer, G. F. Crosta, Y. Pan, R. K. Chang, J. R. Bottiger, *Appl. Opt.* **2004**, *43*, 6198.
[112] J. Neukammer, C. Gohlke, A. Höpe, T. Wessel, H. Rinneberg, *Appl. Opt.* **2003**, *42*, 6388.
[113] G. F. Crosta, S. Zomer, Y.-L. Pan, S. Holler, *Opt. Eng.* **2003**, *42*, 2689.
[114] G. Apostolopoulos, S. V. Tsinopoulos, E. Dermatas, *Biomed. Signal Process. Control* **2013**, *8*, 263.
[115] D. Dannhauser, G. Romeo, F. Causa, I. De Santo, P. A. Netti, *Analyst* **2014**, *139*, 5239.
[116] D. Dannhauser, D. Rossi, F. Causa, P. Memmolo, A. Finizio, T. Wriedt, J. Hellmers, Y. Eremin, P. Ferraro, P. A. Netti, *Lab Chip* **2015**, *15*, 3278.
[117] P. H. Kaye, E. Hirst, R. S. Greenaway, Z. Ulanowski, E. Hesse, P. J. DeMott, C. Saunders, P. Connolly, *Opt. Lett.* **2008**, *33*, 1545.
[118] Z. Ulanowski, E. Hirst, P. H. Kaye, R. Greenaway, *J. Quant. Spectrosc. Radiat. Transfer* **2012**, *113*, 2457.
[119] K. H. Hesselbacher, K. Anders, A. Frohn, *Appl. Opt.* **1991**, *30*, 4930.
[120] N. Roth, K. Anders, A. Frohn, *Appl. Opt.* **1991**, *30*, 4960.
[121] M. Maeda, Y. Akasaka, T. Kawaguchi, *Exp. Fluids* **2002**, *33*, 125.
[122] L. Xie, Y. Yang, X. Sun, X. Qiao, Q. Liu, K. Song, B. Kong, X. Su, *Cytometry, Part A* **2015**, *87*, 1029.
[123] J. Xu, B. Ge, Q. Lu, *Rev. Sci. Instrum.* **2018**, *89*, 123707.
[124] K. B. Aptowicz, R. G. Pinnick, S. C. Hill, Y. L. Pan, R. K. Chang, *J. Geophys. Res.* **2006**, *111*, D12212.
[125] Y.-L. Pan, M. J. Berg, S. S.-M. Zhang, H. Noh, H. Cao, R. K. Chang, G. Videen, *Cytometry, Part A* **2011**, *79A*, 284.
[126] G. F. Crosta, Y.-L. Pan, K. B. Aptowicz, C. Casati, R. G. Pinnick, R. K. Chang, G. W. Videen, *J. Quant. Spectrosc. Radiat. Transfer* **2013**, *131*, 215.
[127] K. B. Aptowicz, Y.-L. Pan, S. D. Martin, E. Fernandez, R. K. Chang, R. G. Pinnick, *J. Quant. Spectrosc. Radiat. Transfer* **2013**, *131*, 13.
[128] O. I. Sindoni, R. Saija, M. A. Iatì, F. Borghese, P. Denti, G. E. Fernandes, Y.-L. Pan, R. K. Chang, *Opt. Express* **2006**, *14*, 6942.
[129] H. Ding, Z. Wang, F. Nguyen, S. A. Boppart, G. Popescu, *Phys. Rev. Lett.* **2008**, *101*, 238102.
[130] W. Choi, C.-C. Yu, C. Fang-Yen, K. Badizadegan, R. R. Dasari, M. S. Feld, *Opt. Lett.* **2008**, *33*, 1596.
[131] Y. Park, M. Diez-Silva, D. Fu, G. Popescu, W. Choi, I. Barman, S. Suresh, M. S. Feld, *J. Biomed. Opt.* **2010**, *15*, 020506.
[132] H. Ding, E. Berl, Z. Wang, L. J. Millet, M. U. Gillette, J. Liu, M. Boppart, G. Popescu, *IEEE J. Sel. Top. Quantum Electron.* **2010**, *16*, 909.
[133] K. Kim, Y. Park, *Opt. Lett.* **2012**, *37*, 4161.
[134] Y. Jo, J. Jung, J. W. Lee, D. Shin, H. Park, K. T. Nam, J.-H. Park, Y. Park, *Sci. Rep.* **2015**, *4*, 5090.
[135] J. Jung, J. Kim, M.-K. Seo, Y. Park, *Opt. Express* **2018**, *26*, 7701.
[136] B. J. Thompson, *J. Phys. E: Sci. Instrum.* **1974**, *7*, 781.
[137] F. C. Cheong, B. Sun, R. Dreyfus, J. Amato-Grill, K. Xiao, L. Dixon, D. G. Grier, *Opt. Express* **2009**, *17*, 13071.
[138] F. C. Cheong, K. Xiao, D. G. Grier, *J. Dairy Sci.* **2009**, *92*, 95.
[139] T. G. Dimiduk, R. W. Perry, J. Fung, V. N. Manoharan, *Appl. Opt.* **2014**, *53*, G177.
[140] T. G. Dimiduk, V. N. Manoharan, *Opt. Express* **2016**, *24*, 24045.
[141] A. Wang, R. F. Garmann, V. N. Manoharan, *Opt. Express* **2016**, *24*, 23719.
[142] J. Fung, R. W. Perry, T. G. Dimiduk, V. N. Manoharan, *J. Quant. Spectrosc. Radiat. Transfer* **2012**, *113*, 2482.
[143] F. Saglimbeni, S. Bianchi, G. Bolognesi, G. Paradossi, R. Di Leonardo, *Soft Matter* **2012**, *8*, 8822.
[144] C. Wang, X. Zhong, D. B. Ruffner, A. Stutt, L. A. Philips, M. D. Ward, D. G. Grier, *J. Pharm. Sci.* **2016**, *105*, 1074.
[145] C. Wang, F. C. Cheong, D. B. Ruffner, X. Zhong, M. D. Ward, D. G. Grier, *Soft Matter* **2016**, *12*, 8774.
[146] M. Gao, P. Yang, D. McKee, G. W. Kattawar, *Appl. Opt.* **2013**, *52*, 5289.
[147] M. J. Berg, S. Holler, *Opt. Lett.* **2016**, *41*, 3363.
[148] M. J. Berg, Y. W. Heinson, O. Kemppinen, S. Holler, *Sci. Rep.* **2017**, *7*, 9400.
[149] T. Kim, R. Zhou, L. L. Goddard, G. Popescu, *Laser Photonics Rev.* **2016**, *10*, 13.
[150] I. Itzkan, L. Qiu, H. Fang, M. M. Zaman, E. Vitkin, I. C. Ghiran, S. Salahuddin, M. Modell, C. Andersson, L. M. Kimerer, P. B. Cipolloni, K.-H. Lim, S. D. Freedman, I. Bigio, B. P. Sachs, E. B. Hanlon, L. T. Perelman, *Proc. Natl. Acad. Sci. U. S. A.* **2007**, *104*, 17255.
[151] B. K. Wilson, M. R. Behrend, M. P. Horning, M. C. Hegg, *Opt. Express* **2011**, *19*, 12190.
[152] V. Richter, F. Voit, A. Kienle, H. Schneckenburger, *J. Microsc.* **2015**, *257*, 1.
[153] T. Wriedt, *J. Quant. Spectrosc. Radiat. Transfer* **2009**, *110*, 833.
[154] G. Gouesbet, G. Gréhan, *Generalized Lorenz-Mie Theories*, 2nd ed., Springer, New York **2016**.
[155] S. Asano, G. Yamamoto, *Appl. Opt.* **1975**, *14*, 29.
[156] A. A. Vinokurov, V. B. Il'in, V. G. Farafonov, *J. Quant. Spectrosc. Radiat. Transfer* **2011**, *112*, 1733.
[157] D. W. Mackowski, *J. Quant. Spectrosc. Radiat. Transfer* **2014**, *133*, 264.
[158] J. Hellmers, V. Schmidt, T. Wriedt, *J. Quant. Spectrosc. Radiat. Transfer* **2011**, *112*, 1679.
[159] K. V. Gilev, E. Eremina, M. A. Yurkin, V. P. Maltsev, *Opt. Express* **2010**, *18*, 5681.
[160] L. Kolokolova, D. Mackowski, *J. Quant. Spectrosc. Radiat. Transfer* **2012**, *113*, 2567.
[161] B. T. Draine, P. J. Flatau, *J. Opt. Soc. Am. A* **1994**, *11*, 1491.
[162] M. A. Yurkin, A. G. Hoekstra, R. S. Brock, J. Q. Lu, *Opt. Express* **2007**, *15*, 17902.
[163] D. I. Podowitz, C. Liu, P. Yang, M. A. Yurkin, *J. Quant. Spectrosc. Radiat. Transfer* **2014**, *146*, 402.
[164] M. I. Mishchenko, J. M. Dlugach, M. A. Yurkin, L. Bi, B. Cairns, L. Liu, R. L. Panetta, L. D. Travis, P. Yang, N. T. Zakharova, *Phys. Rep.* **2016**, *632*, 1.
[165] V. N. Lopatin, N. V. Shepelevich, *Opt. Spectrosc.* **1996**, *81*, 103.
[166] R. S. Brock, X.-H. Hu, D. A. Weidner, J. R. Mourant, J. Q. Lu, *J. Quant. Spectrosc. Radiat. Transfer* **2006**, *102*, 25.
[167] A. E. Moskalensky, D. I. Strokotov, A. V. Chernyshev, V. P. Maltsev, M. A. Yurkin, *J. Biomed. Opt.* **2014**, *19*, 085004.
[168] G. M. Quist, P. J. Wyatt, *J. Opt. Soc. Am. A* **1985**, *2*, 1979.
[169] M. A. C. Potenza, T. Sanvito, S. Argentiere, C. Cella, B. Paroli, C. Lenardi, P. Milani, *Sci. Rep.* **2015**, *5*, 18228.

[170] S. Villa, T. Sanvito, B. Paroli, A. Pullia, B. Delmonte, M. A. C. Potenza, *J. Appl. Phys.* **2016**, *119*, 224901.
[171] M. a. C. Potenza, S. Albani, B. Delmonte, S. Villa, T. Sanvito, B. Paroli, A. Pullia, G. Baccolo, N. Mahowald, V. Maggi, *Sci. Rep.* **2016**, *6*, 28162.
[172] M. A. C. Potenza, L. Cremonesi, B. Delmonte, T. Sanvito, B. Paroli, A. Pullia, G. Baccolo, V. Maggi, *ACS Earth Space Chem.* **2017**, *1*, 261.
[173] B. J. Berne, R. Pecora, *Dynamic Light Scattering: With Applications to Chemistry, Biology, Physics*, Courier Corporation, North Chelmsford, MA **2000**.
[174] L. Cremonesi, A. Passerini, A. Tettamanti, B. Paroli, B. Delmonte, S. Albani, F. Cavaliere, D. Viganò, G. Bettega, T. Sanvito, A. Pullia, M. A. C. Potenza, *Aerosol Sci. Technol.* **2020**, *54*, 353.
[175] C. Feng, L. Huang, J. Wang, Y. Zhao, H. Huang, *Chin. Opt. Lett.* **2011**, *9*, 092901.
[176] R. Liao, P. L. D. Roberts, J. S. Jaffe, *Appl. Opt.* **2016**, *55*, 9440.
[177] B. Sachweh, H. Barthel, R. Polke, H. Umhauer, H. Büttner, *J. Aerosol Sci.* **1999**, *30*, 1257.
[178] V. Filipe, A. Hawe, W. Jiskoot, *Pharm. Res.* **2010**, *27*, 796.
[179] T. Hoshino, M. Itoh, *Opt. Commun.* **2016**, *359*, 240.
[180] I. K. Ludlow, J. Everitt, *Phys. Rev. E* **1995**, *51*, 2516.
[181] A. V. Chernyshev, V. I. Prots, A. A. Doroshkin, V. P. Maltsev, *Appl. Opt.* **1995**, *34*, 6301.
[182] V. P. Maltsev, A. V. Chernyshev, K. A. Semyanov, E. Soini, *Appl. Opt.* **1996**, *35*, 3275.
[183] V. P. Maltsev, V. N. Lopatin, *Appl. Opt.* **1997**, *36*, 6102.
[184] A. J. Patitsas, *J. Colloid Interface Sci.* **1973**, *45*, 359.
[185] N. V. Shepelevich, V. V. Lopatin, V. P. Maltsev, V. N. Lopatin, *J. Opt. A* **1999**, *1*, 448.
[186] S. L. Min, A. Gomez, *Appl. Opt.* **1996**, *35*, 4919.
[187] B. Berge, K. Sudholz, B. Steiner, J. Rohmann, E. Rühl, *Phys. Chem. Chem. Phys.* **1999**, *1*, 5485.
[188] B. Steiner, B. Berge, R. Gausmann, J. Rohmann, E. Rühl, *Appl. Opt.* **1999**, *38*, 1523.
[189] C. Godefroy, M. Adjouadi, *Part. Part. Syst. Charact.* **2000**, *17*, 47.
[190] K. A. Semyanov, P. A. Tarasov, A. E. Zharinov, A. V. Chernyshev, A. G. Hoekstra, V. P. Maltsev, *Appl. Opt.* **2004**, *43*, 5110.
[191] A. V. Chernyshev, P. A. Tarasov, K. A. Semianov, V. M. Nekrasov, A. G. Hoekstra, V. P. Maltsev, *J. Theor. Biol.* **2008**, *251*, 93.
[192] L. Fiorani, V. P. Maltsev, V. M. Nekrasov, A. Palucci, K. A. Semyanov, V. Spizzichino, *Appl. Opt.* **2008**, *47*, 4405.
[193] R. Fantoni, L. Fiorani, A. Palucci, K. A. Semyanov, V. Spizzichino, *J. Optoelectron. Adv. Mater.* **2008**, *10*, 2474.
[194] D. Y. Orlova, M. A. Yurkin, A. G. Hoekstra, V. P. Maltsev, *J. Biomed. Opt.* **2008**, *13*, 054057.
[195] A. V. Romanov, A. I. Konokhova, E. S. Yastrebova, K. V. Gilev, D. I. Strokotov, A. V. Chernyshev, V. P. Maltsev, M. A. Yurkin, *J. Quant. Spectrosc. Radiat. Transfer* **2017**, *200*, 280.
[196] S. Zakovic, Z. Ulanowski, M. C. Bartholomew-Biggs, *Inverse Probl.* **1998**, *14*, 1053.
[197] D. Jakubczyk, G. Derkachov, M. Kolwas, K. Kolwas, *J. Quant. Spectrosc. Radiat. Transfer* **2013**, *126*, 99.
[198] K. V. Gilev, M. A. Yurkin, G. V. Dyatlov, A. V. Chernyshev, V. P. Maltsev, *J. Quant. Spectrosc. Radiat. Transfer* **2013**, *131*, 202.
[199] M. Bartholomew-Biggs, Z. Ulanowski, S. Zakovic, *J. Global Optim.* **2005**, *32*, 325.
[200] A. I. Konokhova, A. A. Rodionov, K. V. Gilev, I. M. Mikhaelis, D. I. Strokotov, A. E. Moskalensky, M. A. Yurkin, A. V. Chernyshev, V. P. Maltsev, *Int. Dairy J.* **2014**, *39*, 316.
[201] D. I. Strokotov, A. E. Moskalensky, V. M. Nekrasov, V. P. Maltsev, *Cytometry, Part A* **2011**, *79*, 570.
[202] M. D. Barnes, N. Lermer, W. B. Whitten, J. M. Ramsey, *Rev. Sci. Instrum.* **1997**, *68*, 2287.
[203] G. V. Dyatlov, K. V. Gilev, M. A. Yurkin, V. P. Maltsev, *Inverse Probl.* **2012**, *28*, 045012.
[204] F. Caramanica, *Prog. Electromagn. Res. M* **2012**, *27*, 109.
[205] R. Charnigo, M. Francoeur, P. Kenkel, M. P. Mengüç, B. Hall, C. Srinivasan, *J. Quant. Spectrosc. Radiat. Transfer* **2012**, *113*, 182.
[206] W. Blohm, *J. Quant. Spectrosc. Radiat. Transfer* **2018**, *208*, 125.
[207] R. O. Duda, P. E. Hart, *Commun. ACM* **1972**, *15*, 11.
[208] M. Hannel, C. Middleton, D. G. Grier, *Appl. Phys. Lett.* **2015**, *107*, 141905.
[209] T. M. Kreis, *Opt. Eng.* **2002**, *41*, 1829.
[210] F. C. Cheong, P. Kasimbeg, D. B. Ruffner, E. H. Hlaing, J. M. Blusewicz, L. A. Philips, D. G. Grier, *Appl. Phys. Lett.* **2017**, *111*, 153702.
[211] D. R. Jones, C. D. Perttunen, B. E. Stuckman, *J. Optim. Theory Appl.* **1993**, *79*, 157.
[212] G. E. P. Box, *Ann. Math. Stat.* **1954**, *25*, 290.
[213] P. G. Moschopoulos, W. B. Canada, *Comput. Math. Appl.* **1984**, *10*, 383.
[214] A. I. Konokhova, D. N. Chernova, A. E. Moskalensky, D. I. Strokotov, M. A. Yurkin, A. V. Chernyshev, V. P. Maltsev, *Cytometry, Part A* **2016**, *89*, 159.
[215] D. N. Chernova, A. I. Konokhova, O. A. Novikova, M. A. Yurkin, D. I. Strokotov, A. A. Karpenko, A. V. Chernyshev, V. P. Maltsev, *J. Biophotonics* **2018**, *11*, e201700381.
[216] M. A. Yurkin, K. A. Semyanov, P. A. Tarasov, A. V. Chernyshev, A. G. Hoekstra, V. P. Maltsev, *Appl. Opt.* **2005**, *44*, 5249.
[217] I. V. Kolesnikova, S. V. Potapov, M. A. Yurkin, A. G. Hoekstra, V. P. Maltsev, K. A. Semyanov, *J. Quant. Spectrosc. Radiat. Transfer* **2006**, *102*, 37.
[218] A. L. Litvinenko, A. E. Moskalensky, N. A. Karmadonova, V. M. Nekrasov, D. I. Strokotov, A. I. Konokhova, M. A. Yurkin, E. A. Pokushalov, A. V. Chernyshev, V. P. Maltsev, *Cytometry, Part A* **2016**, *89*, 1010.
[219] K. V. Gilev, M. A. Yurkin, E. S. Chernyshova, D. I. Strokotov, A. V. Chernyshev, V. P. Maltsev, *Biomed. Opt. Express* **2016**, *7*, 1305.
[220] G. Derkachov, T. Jakubczyk, D. Jakubczyk, J. Archer, M. Woźniak, *J. Quant. Spectrosc. Radiat. Transfer* **2017**, *195*, 189.
[221] A. R. Muliukov, M. A. Yurkin, in *Book of Abstracts of the 17th Conference on Electromagnetic and Light Scattering*, Texas A&M University, College Station, TX **2018**, p. 98.
[222] Z. Ulanowski, Z. N. Wang, P. H. Kaye, I. K. Ludlow, *Appl. Opt.* **1998**, *37*, 4027.
[223] Z. Wang, Z. Ulanowski, P. H. Kaye, *Neural. Comput. Appl.* **1999**, *8*, 177.
[224] V. V. Berdnik, R. D. Mukhamedyarov, V. A. Loiˇko, *Opt. Spectrosc.* **2004**, *96*, 285.
[225] V. V. Berdnik, K. V. Gilev, A. N. Shvalov, V. P. Maltsev, V. A. Loiko, *J. Quant. Spectrosc. Radiat. Transfer* **2006**, *102*, 62.
[226] V. V. Berdnik, V. A. Loiko, *Appl. Opt.* **2009**, *48*, 6178.
[227] V. V. Berdnik, V. A. Loiko, in *Light Scattering Reviews 10*, Springer, Berlin, Heidelberg **2016**, pp. 291–340.
[228] V. V. Berdnik, V. A. Loiko, *J. Quant. Spectrosc. Radiat. Transfer* **2016**, *184*, 135.
[229] V. V. Berdnik, R. D. Mukhamedjarov, V. A. Loiko, *Opt. Lett.* **2004**, *29*, 1019.
[230] V. V. Berdnik, R. D. Mukhamedyarov, V. A. Loiko, *J. Quant. Spectrosc. Radiat. Transfer* **2004**, *89*, 279.
[231] M. V. Klibanov, N. A. Koshev, D.-L. Nguyen, L. H. Nguyen, A. Brettin, V. N. Astratov, *SIAM J. Imaging Sci.* **2018**, *11*, 2339.
[232] M. J. Berg, G. Videen, *J. Quant. Spectrosc. Radiat. Transfer* **2011**, *112*, 1776.
[233] M. J. Berg, N. R. Subedi, *J. Quant. Spectrosc. Radiat. Transfer* **2015**, *150*, 36.

[234] A. Carpio, T. G. Dimiduk, P. Vidal, *SIAM J. Imaging Sci.* **2018**, *11*, 923.
[235] A. Carpio, T. G. Dimiduk, F. Le Louër, M. L. Rapún, *J. Comput. Phys.* **2019**, *388*, 224.
[236] G. David, K. Esat, I. Thanopulos, R. Signorell, *Commun. Chem.* **2018**, *1*, 46.
[237] J. R. Fienup, *Appl. Opt.* **1982**, *21*, 2758.
[238] T. Ekeberg, M. Svenda, C. Abergel, F. R. N. C. Maia, V. Seltzer, J.-M. Claverie, M. Hantke, O. Jönsson, C. Nettelblad, G. van der Schot, M. Liang, D. P. DePonte, A. Barty, M. M. Seibert, B. Iwan, I. Andersson, N. D. Loh, A. V. Martin, H. Chapman, C. Bostedt, J. D. Bozek, K. R. Ferguson, J. Krzywinski, S. W. Epp, D. Rolles, A. Rudenko, R. Hartmann, N. Kimmel, J. Hajdu, *Phys. Rev. Lett.* **2015**, *114*, 098102.
[239] P. C. Chaumet, A. Sentenac, A. Rahmani, *Phys. Rev. E* **2004**, *70*, 036606.
[240] K. Belkebir, P. C. Chaumet, A. Sentenac, *J. Opt. Soc. Am. A* **2005**, *22*, 1889.
[241] P. C. Chaumet, K. Belkebir, R. Lencrerot, *Opt. Express* **2006**, *14*, 3415.
[242] E. Mudry, P. C. Chaumet, K. Belkebir, A. Sentenac, *Inverse Probl.* **2012**, *28*, 065007.
[243] M. T. Bevacqua, R. Palmeri, *J. Imaging* **2019**, *5*, 47.
[244] R. Scapaticci, G. G. Bellizzi, M. Cavagnaro, V. Lopresto, L. Crocco, *Int. J. Antennas Propag.* **2017**, *2017*, 1.
[245] A. Zakaria, C. Gilmore, J. LoVetri, *Inverse Probl.* **2010**, *26*, 115010.
[246] T. Rubæk, P. M. Meaney, K. D. Paulsen, *Int. J. Antennas Propag.* **2011**, *2011*, 1.
[247] S. Coşğun, E. Bilgin, M. Çayören, *Med. Phys.* **2020**, *47*, 3113.
[248] W.-K. Park, *Results Phys* **2020**, *17*, 103071.
[249] K. Kim, K. S. Kim, H. Park, J. C. Ye, Y. Park, *Opt. Express* **2013**, *21*, 32269.
[250] Y. Kim, H. Shim, K. Kim, H. Park, S. Jang, Y. Park, *Sci. Rep.* **2015**, *4*, 6659.
[251] A. Bevan, S. A. Bryant, J. Clark, K. Reid, *J. Aerosol Sci.* **1992**, *23*, 329.
[252] L. Boddy, C. Morris, M. Wilkins, L. Al-Haddad, G. Tarran, R. Jonker, P. Burkill, *Mar. Ecol.: Prog. Ser.* **2000**, *195*, 47.
[253] C. W. Morris, A. Autret, L. Boddy, *Ecol. Modell.* **2001**, *146*, 57.
[254] J. Zhang, G. Wang, Y. Feng, Y. Sa, *J. Biomed. Opt.* **2016**, *21*, 086013.
[255] J. A. Grant-Jacob, B. S. Mackay, J. A. G. Baker, D. J. Heath, Y. Xie, M. Loxham, R. W. Eason, B. Mills, *Opt. Express* **2018**, *26*, 27237.
[256] X. Su, T. Yuan, Z. Wang, K. Song, R. Li, C. Yuan, B. Kong, *Cytometry, Part A* **2020**, *97*, 24.
[257] C. Ding, *J. Quant. Spectrosc. Radiat. Transfer* **2020**, *245*, 106901.

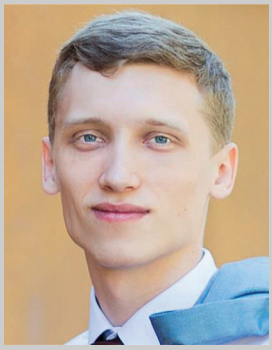

Andrey V. Romanov is a Ph.D. student at the Department of Physics, Novosibirsk State University (Russia). He received his BS and MS degree in physics from Novosibirsk State University in 2016 and 2018, respectively. His current research is focused on the inverse light-scattering problems for single-particle characterization, in particular, spectral methods. More broadly, his research interests range from electromagnetic scattering to deep learning and data analysis.

Maxim A. Yurkin received his BS and MS degrees in physics from the Novosibirsk State University (NSU) with honors (2002, 2004), and dual Ph.D. in computational science and biophysics from the University of Amsterdam and Voevodsky Institute of Chemical Kinetics and Combustion (ICKC, Novosibirsk), respectively (2007). Currently, he is a senior researcher at ICKC and senior teacher at NSU. His research interests include the theory and simulations of electromagnetic scattering, the discrete dipole approximation, and inverse light-scattering problems. He is the main developer of the open-source ADDA code.